Synthesis of bimetallic tungstates for finding photocatalytic active compounds with a smaller band gap than tungsten oxide

Bachelor Thesis

Shinwoo Back

2014 April 11

Supervised under: Kasper Wenderich and Prof. Dr. G. Mul

Committee member: Dr. Arie van Houselt:

ABSTRACT

The goal of the project is to find photocatalytic active tungstates which have a smaller band gap than tungsten oxide (WO_3). Several bimetallic tungstates (MWO_4, M = Cu, Mn, Fe, Ni, Co) have been synthesized by a co-precipitation method and a hydrothermal synthesis method using transition metal salts ($CuCl_2{\cdot}2H_2O$, $MnCl_2{\cdot}4H_2O$, $FeSO_4{\cdot}7H_2O$, $Ni(NO_3)_2{\cdot}6H_2O$, $CoCl_2{\cdot}6H_2O$) and sodium tungstate ($Na_2WO_4{\cdot}2H_2O$) as precursors.

X-Ray diffraction (XRD) analysis and Raman spectroscopy were used to characterize and understand the crystal structure of the as-prepared compounds. Moreover, Scanning Electron Microscopy (SEM) was applied to study the form of the most photocatalytic active compound, $MnWO_4$. UV–Visible diffuse reflectance spectroscopy is also used to measure the band gap of each material.

After the characterization of each compound, several photodegradation experiments were done to observe the photocatalystic activity. Under the UV light, the experiment was followed by changing one parameter per time to attain higher sensitivity of the photocatalyst. Concluding, after the experiment under the visible light, the $MnWO_4$ was found out to be most photocatalytic active with a smaller band gap than tungsten oxide

Table of Contents

1. Introduction

1.1. Introduction to photocatalysis

The exhaustion of fossil fuels is one of the most urgent problems these days. A lot of research is put into renewable energy such as wind energy and solar energy.[5] Despite the fact that these technologies are considered to be technically reliable, they do not meet the economical standards.[6] This has hindered the application of these promising techniques over the past few years. The interest and demand for getting highly efficient materials among researchers and industry are rising. [7]

The expectation is that one of the most promising solutions, which is the water splitting technology, could reach a solar-to-hydrogen Ratio of 10 % within 10 years.[8] Currently, this is the main driving force for more investments in the technology since it has the same order of magnitude of the ratio as current solar panels. Water splitting technology has several opportunities to increase the total efficiency. The methods of enhancing the sensitivity of the materials are discussed in following chapter 1.2.

The basic principle of the photocatalysis can be described with an example method, which is the water splitting technology.[9] Band gap is the energy gap between the conduction band (C.B.) and the valence band (V.B.). (Fig. 1.1.1, left) General water splitting occurs when the conduction band of the material is higher than that of reduction potentials (0 eV) and the valence band of the material is lower than that of oxidation potentials (1.23 eV). As the light is absorbed by the material, the electrons are emitted from valence band, leaving a hole behind. This electron can only be promoted to conduction band if the light has equal or higher photon energy than the band gap of the material. Reduction of the H^+ ions to H_2 occurs by the electrons in the conduction band, while the oxidation of H_2O to O_2 occurs by the holes in the valence band. Catalysts with smaller band gaps can absorb the light in higher wavelengths and thus active in a larger part of the solar spectrum. (Fig. 1.1.1, right) Therefore, finding the material which has a smaller band gap is one of the main concerns.

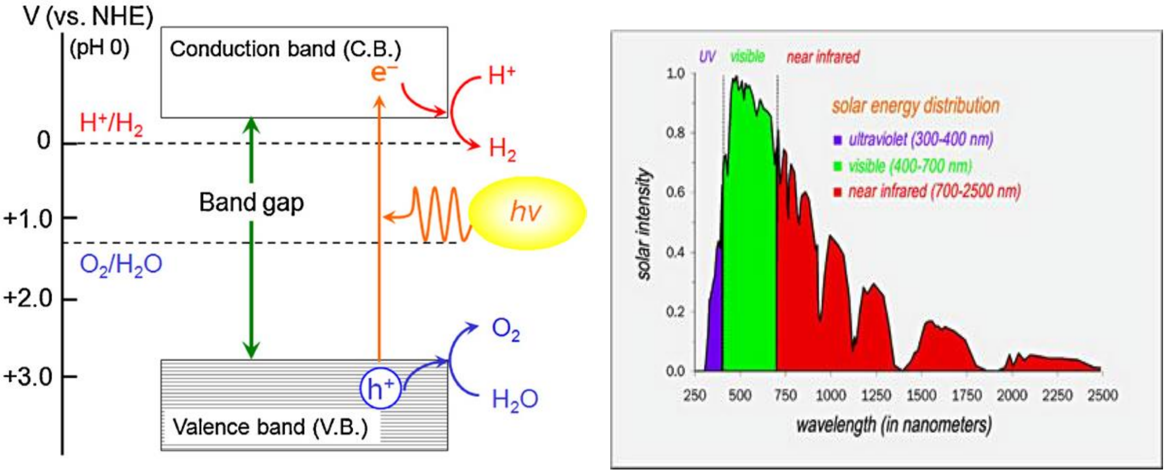

Figure 1.1.1. Schematic of photocatalytic activity[10] (left) and visible light spectrum (right)[11]

Z-scheme is one of the techniques of water splitting technology which is studied in PCS group as the following:[8] Water splitting occurs in the presence of sunlight. A metallic membrane is put in the water in such a way that the sunlight reacts on both sides of it. On either side of the membrane catalysts are placed, one for oxygen evolution on one side and one for hydrogen on the other. In a catalytic reaction with protons and electrons, hydrogen is formed, in another catalytic reaction with water and electron holes, oxygen and protons are produced. The transport of electrons through the metallic membrane and protons through a small gap underneath the membrane ensures the ongoing process of reactions. The hydrogen and oxygen – both gasses – bubble up on separate sides of the membrane.

1.2. Challenges and Opportunities

In order to improve the sensitivity of photocatalysts towards higher wavelength, the stability and cost have to be taken into account. Therefore, identifying new materials which have good efficiency, stability and availability is important.

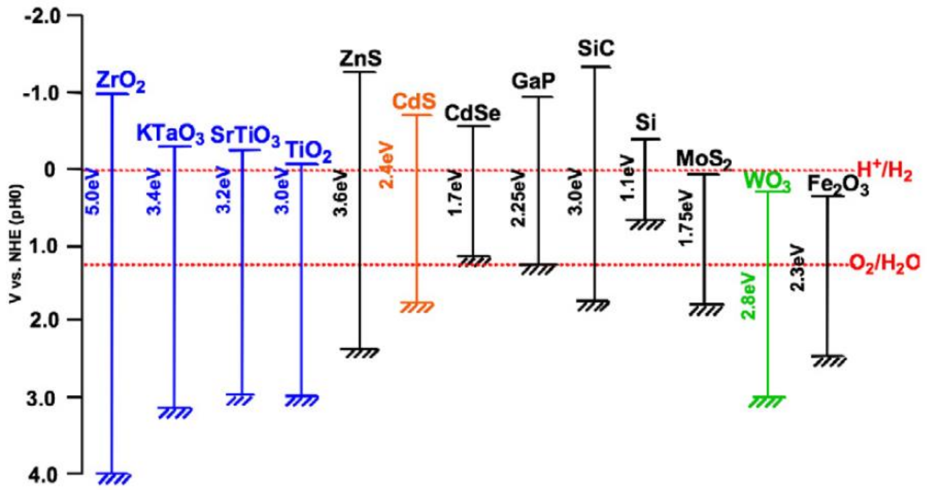

Figure 1.2.1. Various kinds of semiconductors with different band gap

1.2.1 Choosing WO_3 as reference semiconductor

The energy band configuration is one of the most important fundamental properties which has to be considered. It determines the absorption of incident photons, the resulting photoexcitation of electron-hole pairs and the redox capabilities of excited-state electrons and holes. Therefore, finding indirect and narrow band gap semiconductors is important. The photocatalyst which exhibits high absorbance under visible light spectrum would be more suited for the efficient harvesting of low energy photons under the part of solar spectrum.

Tungsten oxide (WO_3), which is well known as one of the most promising photocatalysts,[3] was chosen for reference compound. (Fig. 1.2.1.) It also meets the criteria mentioned in the beginning of this chapter. According to literature by Rajagopal et al, the tungstates have several interesting properties which gain attention by having various types of technological applications such as microwave, scintillation, optical modulation, magnetics and writing-reading-creasing devices, humidity sensors, optical fibers and photoluminescence materials.[3]

All in all, it is important to synthesize different tungstates correctly and verify if they show any photocatalytic activity through dye photodegradation experiments. The promising catalysts can be tested to see if there is a difference in photocatalytic activity under visible light. The aim of the research is to find the best photocatalyst MWO_4 compound which can absorb light with a higher wavelength than WO_3 and has band gap smaller than WO_3.

1.2.2 Enhancing the sensitivity of the photocatalyst towards higher wavelengths

In order to enhance the sensitivity of the photocatalyst, there are several methods to tackle the problem. Before starting with the discussion, one should be informed that the method of comparing different W-based binary oxide semiconductors is already a method which was chosen for enhancing the efficiency by narrowing band gap for photocatalysts with higher wavelengths. Research has been done with binary tungstates, ternary tungstates and WO_3 – based combined photocatalysts.[12] In this report, binary tungstates are investigated.

The first method, doping, consist of modifying the band gap and band positions of WO_3 by introducing a new element in the crystal lattice. In this experiment, doping was not performed.

As mentioned in the introduction chapter as an example of a water splitting technology, there is also a promising method called Z-scheme method which combines two different semiconductors for better selectivity. This method is being researched on by PCS group at University of Twente.[8] Once the material with a small band gap is found, it can be incorporated in such a Z-scheme.

1.2.3 Increasing the photocatalytic activity

To begin with, cocatalysts can be utilized in order to separate electrons and holes effectively in photocatalyst materials without recombination. They act as a beacon for either electrons or holes. In this research, Pt was chosen as a cocatalysts which acts as an electron scavenger.[13]

Furthermore, in order to control the shape of the compounds, capping agents could be used. The characteristics and properties of surface/interface plays a great role between photocatalyst and reactant. It mainly effects the transfer of electrons and energy between substances, governing selectivity and determining the susceptibility of the photocatalyst toward photo corrosion. Some facets are more stable than others, and these high-energy facet could be deliberately fabricated for better performance.[14]

1.3. Procedure of the experiment

In this work, multiple bimetallic tungstates (MWO_4, M=Cu,Mn,Fe,Ni,Co) were synthesized by a co-precipitation and a hydrothermal synthesis method. The X-ray diffraction (XRD) patterns were measured after the synthesis and then compared with the literature to check if the right compound has been synthesized. In addition to XRD, to understand more about the materials, Raman spectroscopy and Scanning Electron Microscopy (SEM) were applied to see the composition and the shape of the compound, respectively. SEM was only used for $MnWO_4$ not only because of the high cost and the time it takes for an experiment, but also because it was the only promising compound out of all synthesized compounds in regards of its photocatlytic activity. UV–Visible diffuse reflectance spectroscopy was used to measure the band gap of each material.

Photodegradation experiments were done afterwards using a box reactor with UV–visible spectroscopy to observe photodegradation of the dye Acid orange 7 (AO7) under a wavelength of 375 nm of ultraviolet (UV) light to test the as-prepared photocatalysts.

At first, the original compounds which were synthesized at 400 ℃ were examined. Later on, the samples synthesized at 400 ℃ were calcined again at 550 ℃ and 700 ℃. The samples calcined at 700 ℃ were tested as well through photodegradation experiments. From the group of compounds which were calcined at 550 ℃, only $MnWO_4$ was examined in order to compare the photocatalytic activity at different calcination temperatures.

In order to enhance the photocatalytic activity, additional impregnation of Pt was done only on commercial WO_3 and the three most photocatalytic active samples, which were $CuWO_4$, $MnWO_4$ and $NiWO_4$.

At the end, the best six samples, WO_3 with and without Pt, $MnWO_4$ with and without Pt, $CuWO_4$ and $NiWO_4$, were chosen according to their photocatalytic activity. Then the photodegradation experiment was done with visible light under a wavelength of 447 nm (violet lamp) instead of UV light.

Additionally, $CoWO_4$ was synthesized and tested at the end of the project. It showed less activity compared to all the other samples in the photodegradation experiments. Also, due to a lack of time, band gap measurements and Raman spectroscopy were not performed for this compound.

2. Theoretical Aspects

2.1 Characterization

2.1.1. X-Ray Diffraction (XRD)

XRD can be applied to study crystal structures. A crystal is constructed by the numberless repetition in space of identical 'building blocks'. When diffraction occurs at a certain angle, there might be interference. As the waves interact with an object, optical diffraction occurs. Bragg Reflection equation is used.

$$n\ \lambda = 2d \sin \theta$$

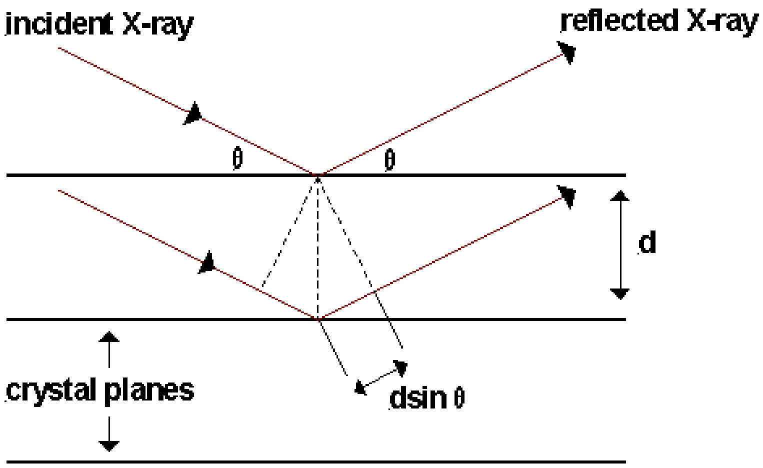

Figure 2.1.1. Schematic of Bragg Reflection.[15]

λ is given by the wavelength of the X-ray beam and θ is measured from the reflection angle. d is the spacing between the lattice planes. This is also depicted in the Figure 2.1.1.

For a crystal, the beam is reflected to the detector only when the crystal is correctly oriented. Only a few crystallites have the right orientation in normal powder sample.[16] Other crystallites meet the diffraction condition as the tilt angle changes. In such a case, single crystal diffraction is used for investigating the crystal structure. Polycrystalline (powder) diffraction is applied for determination of the structure itself, or for determination of structure related properties, such as the phase identification and quantification, residual stress, texture, etc.

The purpose of this analysis is to determine and compare the crystalline phases of the sample. To do this, the measurements are compared with patterns in a reference database. Through phase identification you can find which phases from the reference database are present in the sample.

In conclusion, the diffraction pattern could be represented as a fingerprint of the crystal structure. Also, the location of the peaks in the XRD pattern indicate the position and type of atoms/molecules in the unit cell.

2.1.2. Raman spectroscopy

Raman spectroscopy is a spectroscopic technique which is employed to examine the frequencies present in the radiation scattered by molecules.[17] Then the differences in molecular states are determined. When one in millions of the incident photons collides with the molecules, it gives up some of the energy and is emitted with other lower energy. Lower frequency Stokes radiation from the sample (Fig. 2.1.2.) is formed from these scattered photons. Higher frequency anti-Stokes radiation occurs when the other incident photons collect energy from the excited molecules. Rayleigh radiation is composed when the component of radiation is scattered without change of frequency. Furthermore, vibrational and rotational transitions are observed through analysis of radiation scattered by molecules in Raman spectroscopy. By measuring the net absorption of infrared radiation and microwave radiation, vibrational transitions and rotational transitions are observed, respectively.

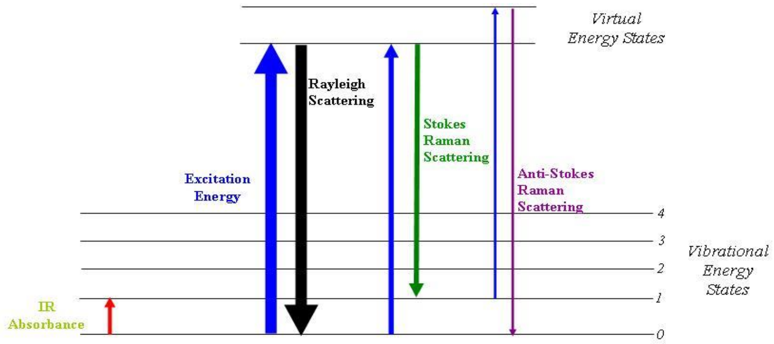

Figure 2.1.2. Schematic of Raman spectroscopy.[18]

2.1.3. Band gap determination

To determine the band gap of the compounds, UV-Vis diffuse reflectance spectra of the samples have to be measured first. Out of these data, the reflectivity R can be calculated. The Kubelka-Munk function F(R) is required for obtaining the band gap. The Kubelka-Munk equation is expressed as follows:

$$F\ (R) = \frac{(1-R)2}{2R}$$

After reflectance spectrum is converted to Kubelka-Munk function, the Kubelka-Munk plot is made by plotting F (R) on the y-axis. The wavelength is plotted on the X-axis.

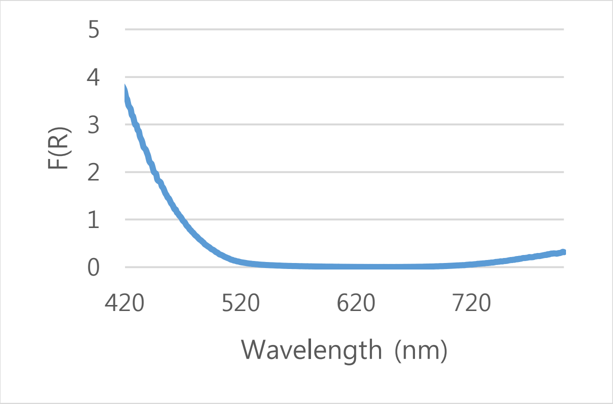

Figure 2.1.3. Kubelka-Munk plot of $CuWO_4$

Out of the Kubelka-Munk plot, the Tauc plot can be calculated. To do so, $(hv\ F(R))^{1/2})$ =is plotted on the y-axis. The energy in electron volts(eV) (hv = 1239.7/λ) is plotted on x-axis.

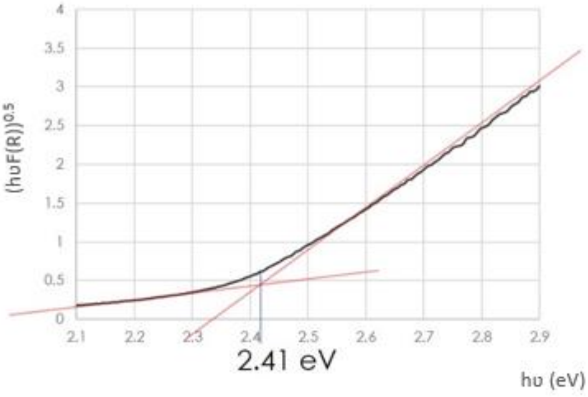

Figure 2.1.3. Tauc Plot of $CuWO_4$

An example of measuring the band gap from Tauc plot is shown above. (Fig. 2.1.3.) Tauc indication values, which can be calculated by the method which was mentioned earlier, are plotted on the y-axis accordingly with hV (eV) on the x-axis. The steepest slope and the gentlest slope is drawn. Then, a vertical line is drawn from the intersection of these two slopes. The value which one reads from the intersection with the x-axis is the band gap of the compound. This is how the band gap of $CuWO_4$ of 2.41 eV was measured from Tauc Plot. [19,20]

2.2 Dye photodegradation

Dye photodegradation is a method to test if a photocatalyst exhibits photocatalytic activity. A dye is degraded through either oxidation or reduction. For a dye to be photocatalytically oxidized, the oxidation potential should be above the valence band of the photocatalyst. Reduction occurs when the reduction potential is below the corresponding conduction band of the photocatalyst. The Lambert-Beer law is applied to calculate the dye concentration by measuring the spectrum of the reaction mixture. It states that the absorbance of the dye solution is proportional to the dye concentration. Therefore, the decrease of concentration over time is calculated with this derivation and this data is later on used to determine the photocatalytic activity of the catalyst. O_2 could be replaced by Fe^{3+} as a more suitable reducing agent.

3. Experimental Aspects

3.1. Preparation of Samples

For the preparation of samples, the amount of chemicals was chosen in accordance with the amount which was used from the literature by García-Pérez et al.[2] The synthesis method was also inspired by this paper. All the MWO_4 (M = Cu, Mn, Ni, Co) compounds except $FeWO_4$ were synthesized by a co-precipitation method. $FeWO_4$ is the only material which was synthesized by the hydrothermal synthesis method. First, solution A, which contained 0.00963 mol of transition metal precursor ($CuCl_2 \cdot 2H_2O$, $FeSO_4 \cdot 7H_2O$, $Ni(NO_3)_2 \cdot 6H_2O$, $CoCl_2 \cdot 6H_2O$), was diluted in 15mL of distilled water. Solution B was prepared afterwards, containing 0.00963 mol of $Na_2WO_4 \cdot 2H_2O$ with 25mL of distilled water. Ranging from a stirring speed of 300 rpm to 500 rpm, solution A and solution B were stirred for 20 min separately. Solution A was then added drop-wise into solution B while the latter was retained at the same stirring speed. The desired solution was then stirred for at least 20 min and up to 3 hours to form a residue. To separate liquid and residue, the solution was centrifuged at 8500 rpm for 30 minutes. Two additional centrifuging steps followed, with the same speed, for washing. This was done to eliminate remainings such as nitrate, chloride, and sodium ions from the synthesis procedure. After separating the residue from the solution by centrifugation for 30 min, the residue was washed by adding Millipore water and centrifuging again for 20 minutes. Subsequent to separation of the residue from the solution, additional washing took place with ethanol using the same procedure. After centrifuging, the sample was put into ceramic bowl for drying. Drying was done at 90 ℃ for 24 hours. Calcination in air was followed accordingly and done at 400 ℃ for 24 hours. A detailed description table can be found in Appendix chapter 7.8.

3.2. Characterization of Samples

In this chapter, all the parameters used for characterization of samples can be seen in the tables. XRD, Raman spectroscopy and UV-visible diffuse reflectance spectroscopy were measured with the programs from the computer for the characterization.

For measuring XRD patterns, a Bruker D2 Powder XRD machine was used.

Scan type	Time	Steps	2Theta Start	2Theta Increment	2Theta Stop	Auto repeat	Variable rotation
Coupled Two Theta/Theta	1s	1187	10°	0.05°	70°	2 times	10/min

Table 3.2.1. Parameters for the XRD

For Raman spectroscopy, Bruker Senterra Raman Spectrometer machine was employed.

Wavelength	Power	Dimension	Length
532nm	5mW	1200ab	3-5cm

Table 3.2.2. Parameters for the Raman spectroscopy

UV-visible diffuse reflectance spectroscopy was carried out for investigating the band gap of each material. In this experiment, samples were first transferred onto a DRIFT-cell (Harrick, Praying Mantis). $BaSO_4$ was used as the reference substrate. In order to determine the optical band gap, the Tauc equation which was mentioned from the previous chapter was applied.

Data mode	PMT Gain	Starting wavelength	Stop wavelength	Bandwidth	Scan Speed	Data Interval	Lamp Change	Cycles
Intensity	100	400 nm	600 nm	2 nm	240 nm/min	1 nm	325 nm	1

Table 3.2.3. Parameters for the UV-visible diffuse reflectance spectroscopy.

3.3. Photocatalytic reaction of Samples

To test the photocatalytic activity of the synthesized samples, beakers were prepared containing 50 mL of 0.15 mM Acid orange 7 (AO7). AO7 solution is provided with air by a tube for about an hour to provide oxygen for the reduction before the experiment. 25 mg of MWO_4 were added to the solution afterwards. Each prepared beaker is then put into box reactor (Fig. 3.3.1.) with a stirring speed of 500 rpm in the dark for an hour. Two minutes after the beginning of illumination, measurements are done every 30 min. First sample of 3 mL is pipetted out at t = 0 min. Then the samples of 2 mL are pipetted out again at t = 0min and afterwards, solution of 2 mL is pipetted out every 30 minutes. After two hours of exposure under the light, two more measurements were taken every hour in a same condition. The very first measurement at t = 0 min was discarded afterwards. All in all, 7 measurements are done in 5 hours.

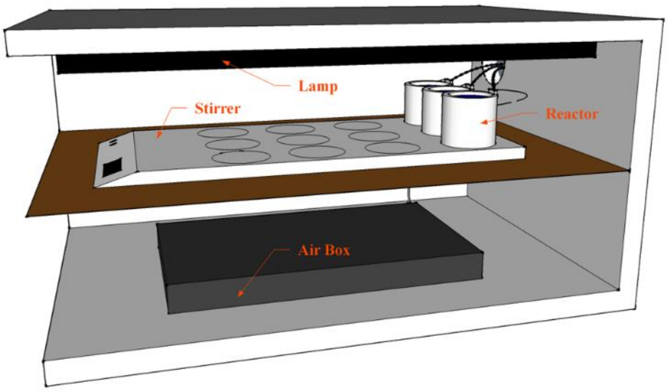

Figure 3.3.1. Schematic of the Box Reactor, drawn by Romao.

UV/Vis spectroscopy measures the relative change of transmittance of light as it passes through a solution. Then the absorbance is calculated throughout this measurement, using the Lambert-Beer law. The baseline was first measured using water. All the parameters were set to the data which can be seen in Table 3.3.1.

Data mode	Starting wavelength	Stop wavelength	Bandwidth	Scan Speed	Data Interval	Lamp Change	Cycles
Absorbance	400 nm	600 nm	2 nm	240 nm/min	1 nm	325 nm	1

Table 3.3.1. Parameters for the UV/Vis spectroscopy

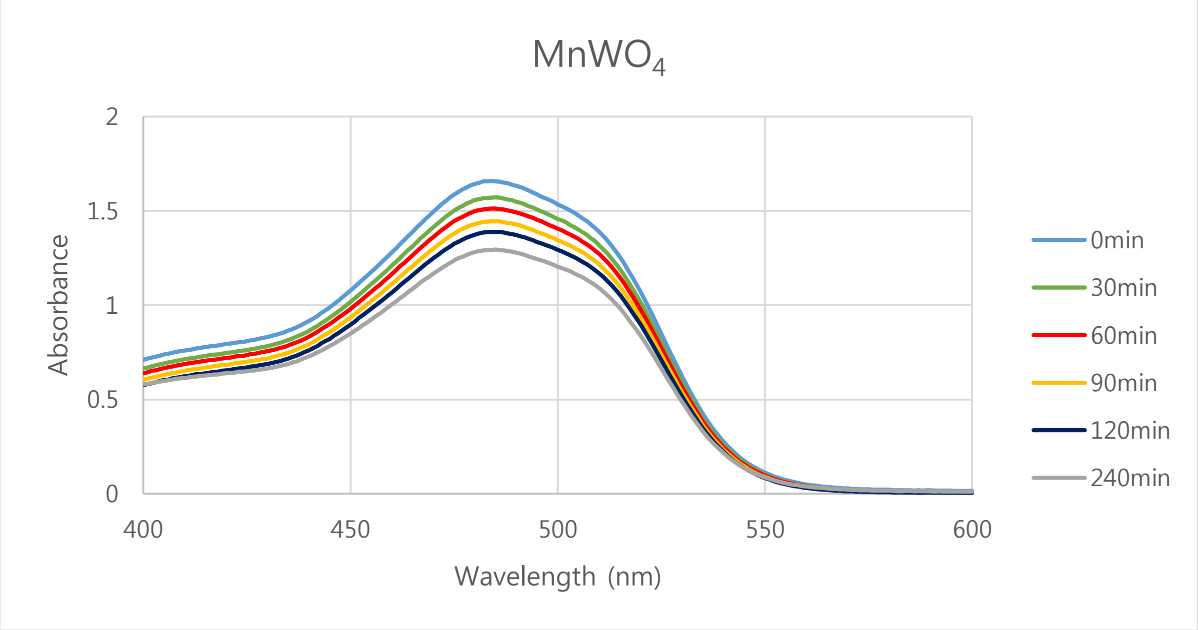

Figure 3.3.2. Light absorbance of 0.15 mM of AO7 with $MnWO_4$ *under UV light.*

An example which shows light absorbance of 0.15 mM of AO7 is demonstrated above. (Fig. 3.3.2.) It can be seen that the absorbance curve decreases over time.

The highest peak, at 484nm in each case, was chosen and the ratio of the absorbance difference at that point was applied to draw the graphs on chapter 4.5.

Reaction kinetics for WO_3 follow the 1^{st} order kinetics and it was assumed that it would be similar for the rest of the compounds as well for all the photodegradation experiments. [Wenderich and Mul, submitted] This is expressed as dotted lines in the upcoming figures in chapter 4.5. Photodegradation measurements.

4. Measurement Results and Discussion

4.1. XRD Comparison

4.1.1. Samples calcined at 400 ℃

The results obtained from the profiles of the XRD patterns generally agree with those of the literature values. The peaks correspond mostly with the theoretical results. One general remark is that after $2\theta=40^{o}$, peaks were difficult to distinguish.

However, when $FeWO_4$ was synthesized by co-precipitation method, it did not show the right pattern compared to literature.[3] Therefore, $FeWO_4$ was re-synthesized by performing a hydrothermal synthesis method instead. Still, the patterns of $FeWO_4$ correspond with the literature profiles the least out of all MWO_4 (M = Cu, Mn, Fe, Ni, Co), showing the profile with a lot of noise. (Fig. 4.1.3.)

4.1.2. Samples calcined at 550 ℃ and 700 ℃

After synthesizing MWO_4 (M = Cu, Mn, Fe, Ni, Co) at 400 ℃, all the compounds were calcined again at 550 ℃ and 700 ℃ for 12 hours. All the compounds which were calcined at 700 ℃ showed the best crystallinity shape. XRD patterns of these samples sometimes showed sharper and higher peaks than the samples synthesized at 400 ℃, which was difficult to be determined in the beginning. Sometimes the intensity got higher, resulting in lengthening of the height of the peak. In general, as the calcination temperature rises, the conclusion was reached that compounds showed better crystallinity within the range of 400 ℃ to 700 ℃. The comparison of XRD patterns from literature and synthesized compounds are discussed individually under the figures.

4.1.3. Comparison between literature and synthesized compounds.

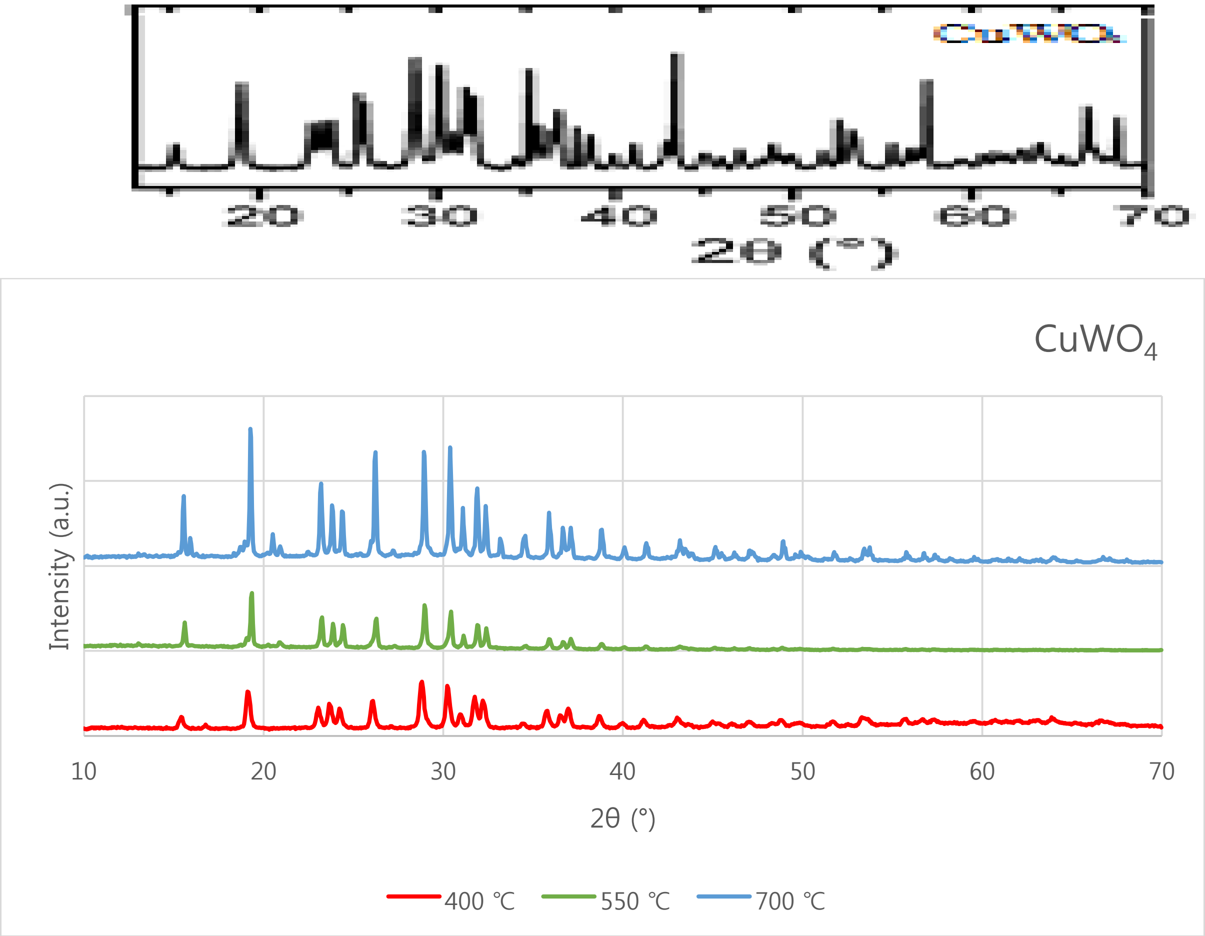

Figure 4.1.1. XRD pattern comparison of $CuWO_4$ between literature figure[4] (top) and synthesized ones at different temperatures (bottom)

As the temperature rises, the peaks became sharper and higher. Therefore, $CuWO_4$ showed better crystallinity as the calcination temperature rose. More peaks were observed at the higher temperatures as well.

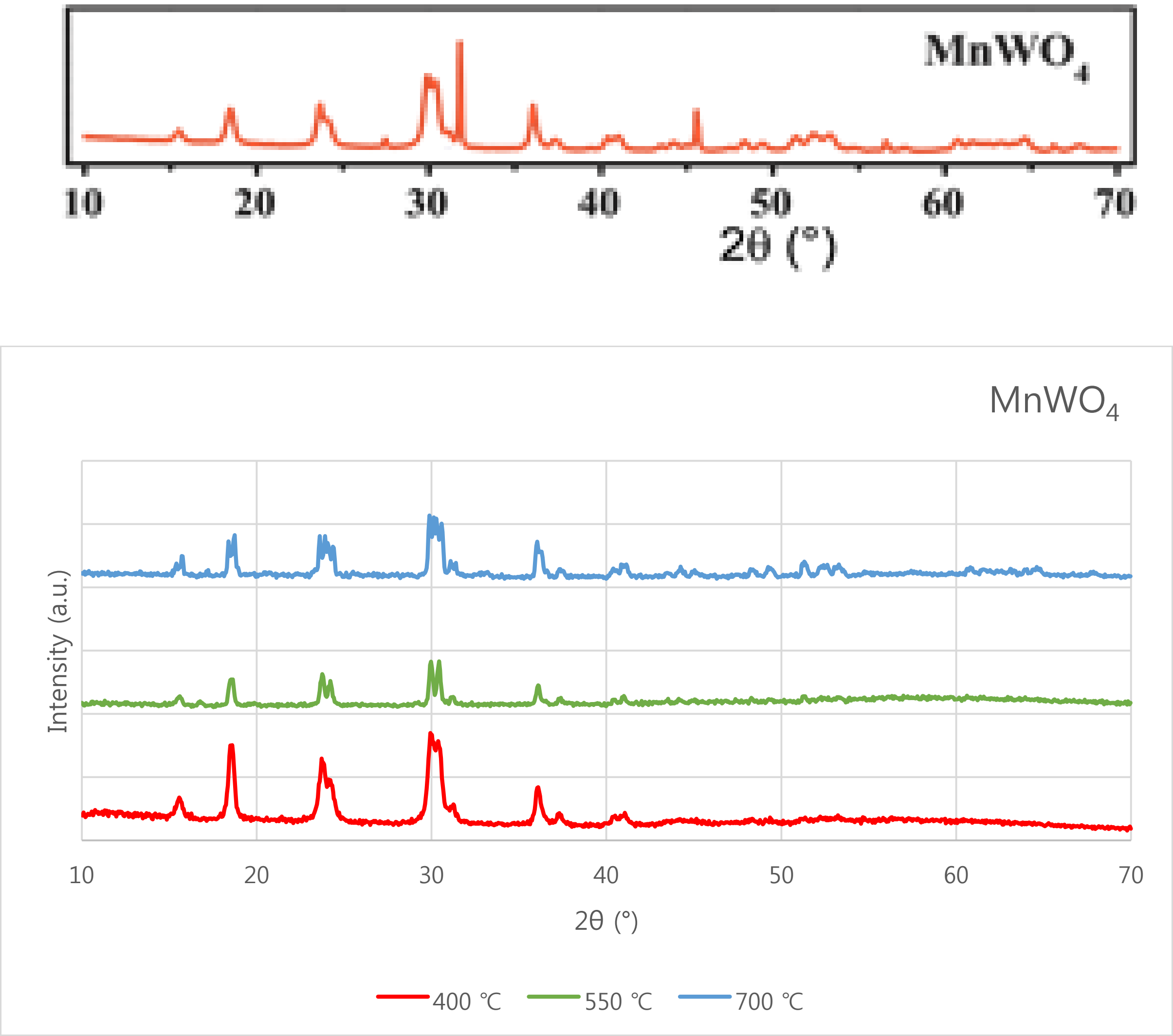

Figure 4.1.2 XRD pattern comparison of MnWO$_4$ between literature figure[2] (top) and synthesized ones at different temperatures (bottom)

The location of the measured lines are in correspondence with the literature figure until 2θ = 45°. Unlike the other figures in this chapter, the compound which was originally synthesized at 400 ℃ showed better crystallinity than the other two samples.

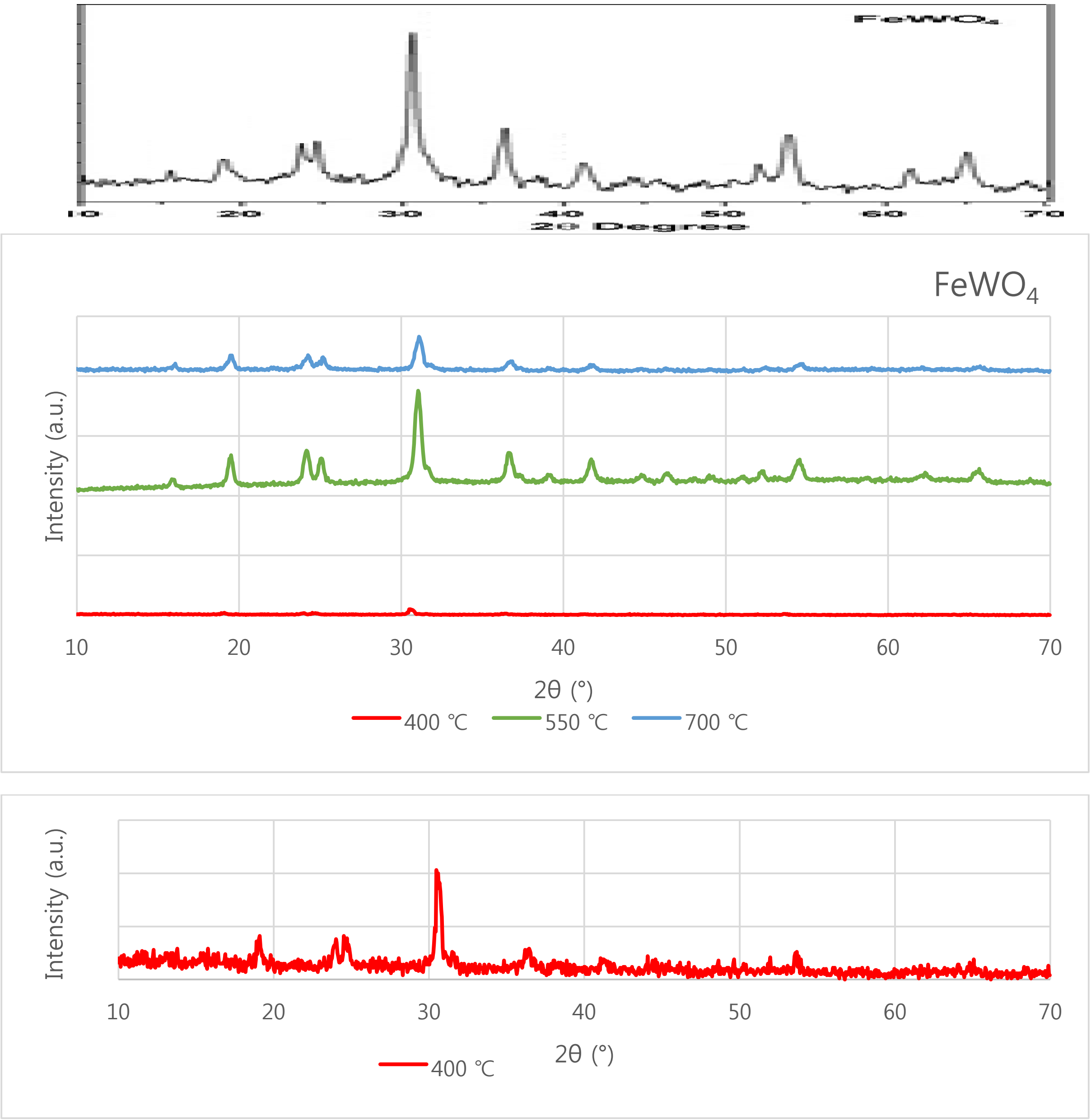

Figure 4.1.3. XRD pattern comparison of $FeWO_4$ between literature figure[3] *(top) and synthesized ones at different temperatures and a zoomed-in version at 400 ℃. (bottom)*

A drastic change in intensity was observed when additional calcining was treated to the compound. The XRD pattern of the originally synthesized compound shows really low intensity with a lot of noise. This as-prepared $FeWO_4$ has very low crystallinity.

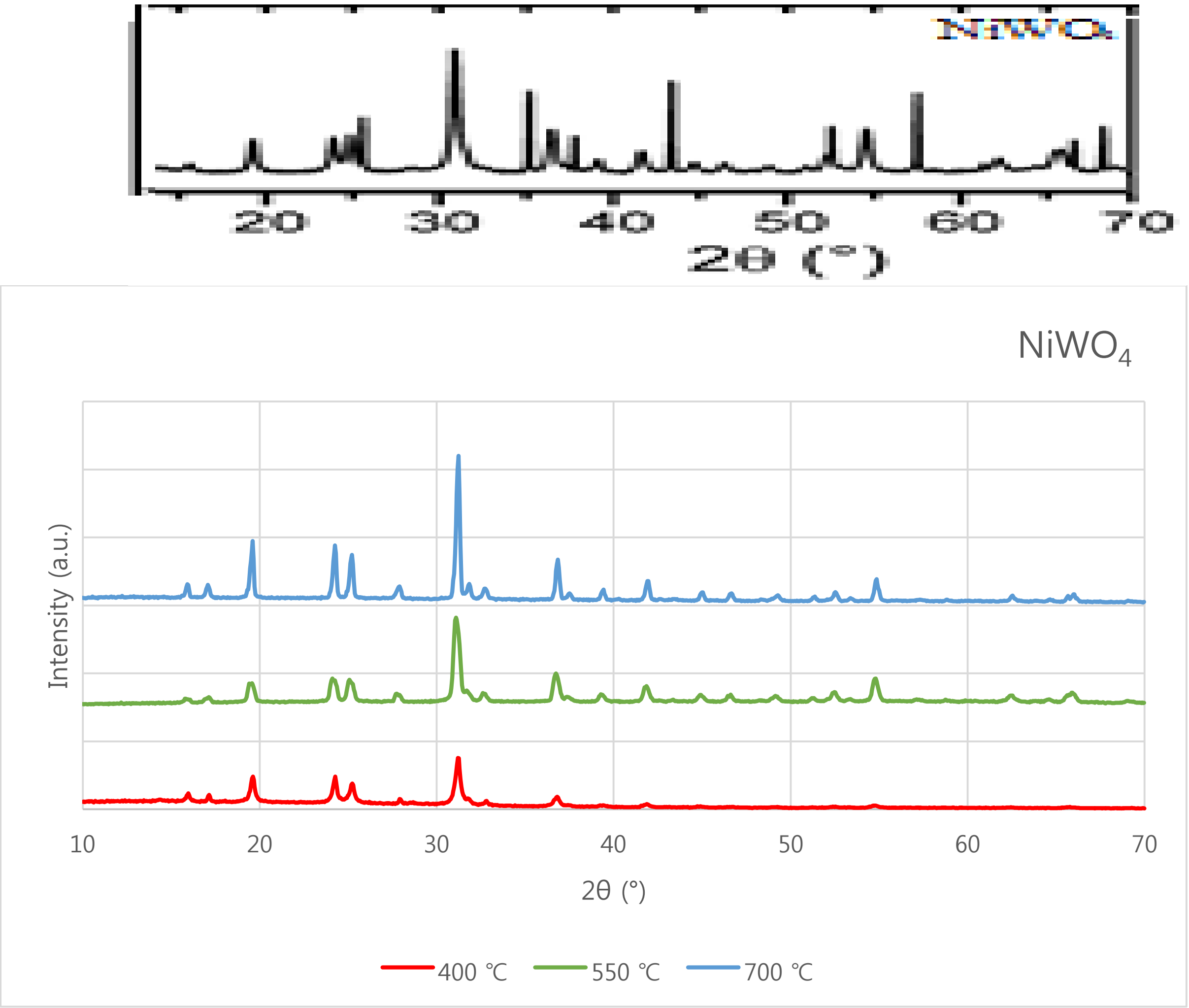

Figure 4.1.4. XRD pattern comparison of NiWO$_4$ between literature figure[4] *(top) and synthesized ones at different temperatures (bottom)*

In 2θ = 28°, the peak was shown in our measured data, while it was not shown in the literature figure. When calcined at 550 ℃ and 700 ℃, additional peaks were observed after 2θ = 45°. There are several one-lined peaks in the literature figure, which can be treated as defects measured by the authors.

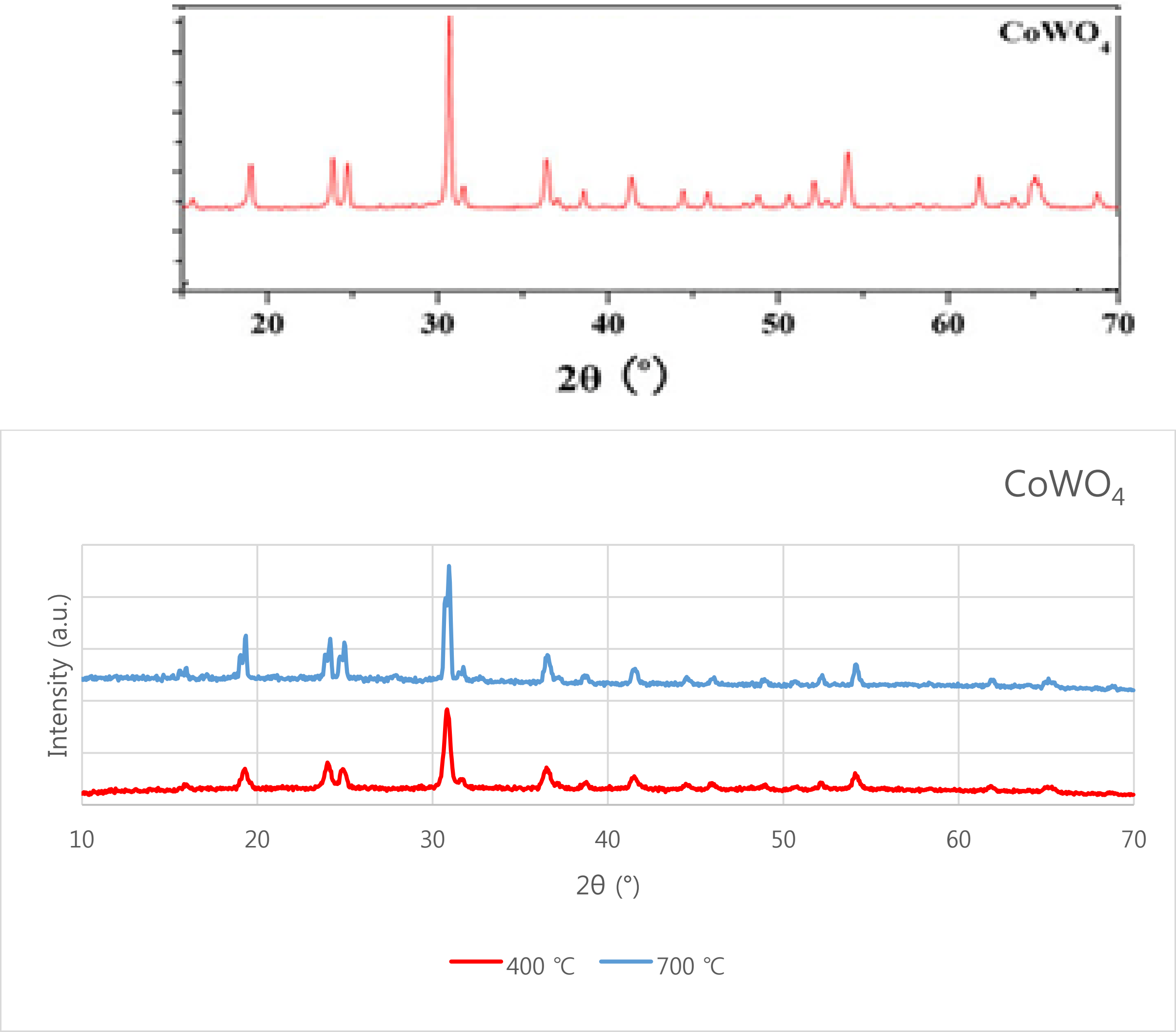

Figure 4.1.5. XRD pattern comparison of $CoWO_4$ between literature figure[1] (top) and synthesized ones at different temperatures (bottom)

The location of the measured lines match mostly with those of the literature values. The reason why 550 ℃ line is missing for the case of $CoWO_4$ is that it was only calcined at 700 ℃ after the synthesis. The peaks became sharper and higher as the temperature rises as well. Therefore, $CoWO_4$ showed better crystallinity as the calcination temperature rose.

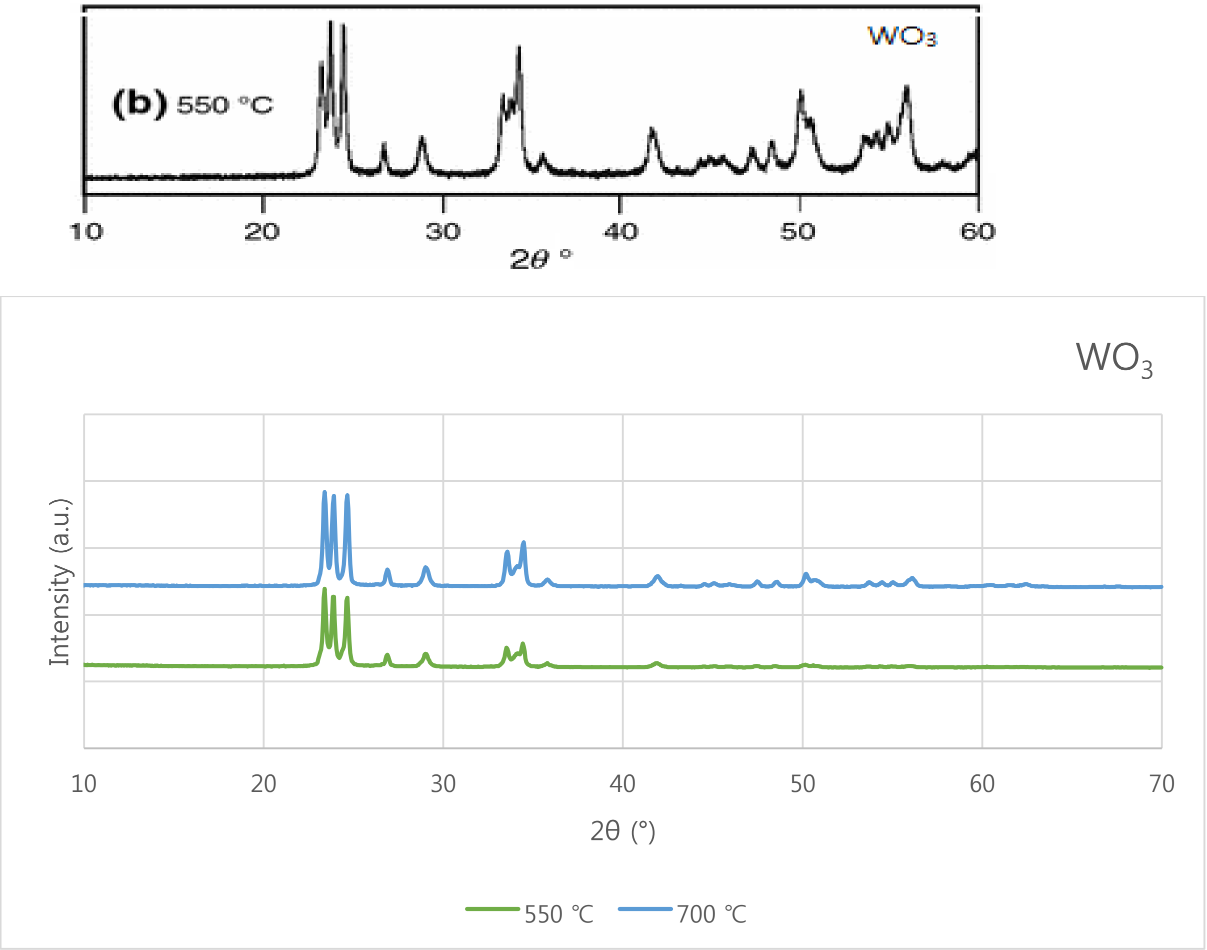

Figure 4.1.6. XRD pattern comparison of WO_3 between literature figure[21] *(top) and synthesized ones at different temperatures (bottom)*

Commercial WO_3 was calcined at 550 ℃ and 700 ℃. The location and the curve of the measured lines are corresponding greatly with the literature figure until 2θ = 45°. However, after 2θ = 45°, it was difficult to distinguish the peaks from measured XRD patterns.

4.2. Raman Spectroscopy

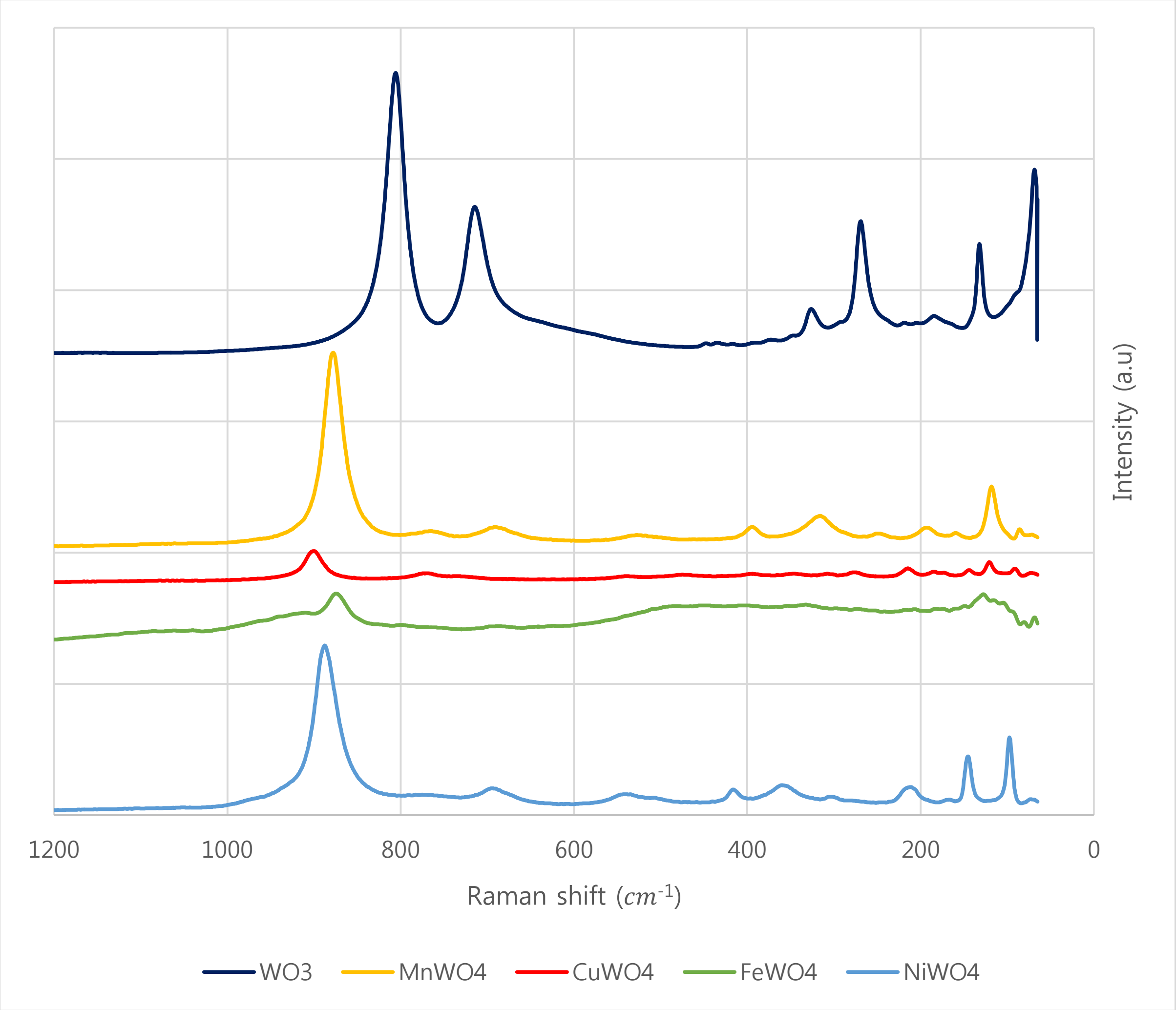

Figure 4.2.1. Raman spectroscopy comparison with all MWO_4 with WO_3. Only for the intensity value of WO_3 was divided by 10 for better comparison.

Raman spectra of the measured compounds can be found in Figure 4.2.1. From the figure, one could tell that 'WO' bond is located on around $900cm^{-1}$. When compared with WO_3, the WO bond seems to be shifted for the MWO_4 (M = Cu, Mn, Fe, Ni) samples. While $FeWO_4$ was showing low intensities due to its less crystallinity, low intensity of the peaks were also observed from $CuWO_4$. It was unexpected since it showed great crystallinity when XRD patterns was measured.

4.3. Band gap Measurements

Compounds	$CuWO_4$	$MnWO_4$	WO_3	$FeWO_4$	$NiWO_4$
Band gap (eV)	2.41	2.5	2.65	Unavailable	Unavailable

Table 4.3.1. The band gaps of different tungstates (MWO_4, M = Cu, Mn, Fe, Ni, Co).

The measured band gap of each compound can be seen on Table 4.3.1. For the case of $FeWO_4$ and $NiWO_4$, it was difficult to determine the band gap of the material due to a lot of noise in the graph. Measurement methods are described through chapter 2.1.3. The measured Tauc plot of $CuWO_4$ (Fig. 2.1.3.) is one of the best measurement data and the other Tauc plots are in the Appendix chapter 7.1.

4.4. Scanning Electron Microscopy (SEM)

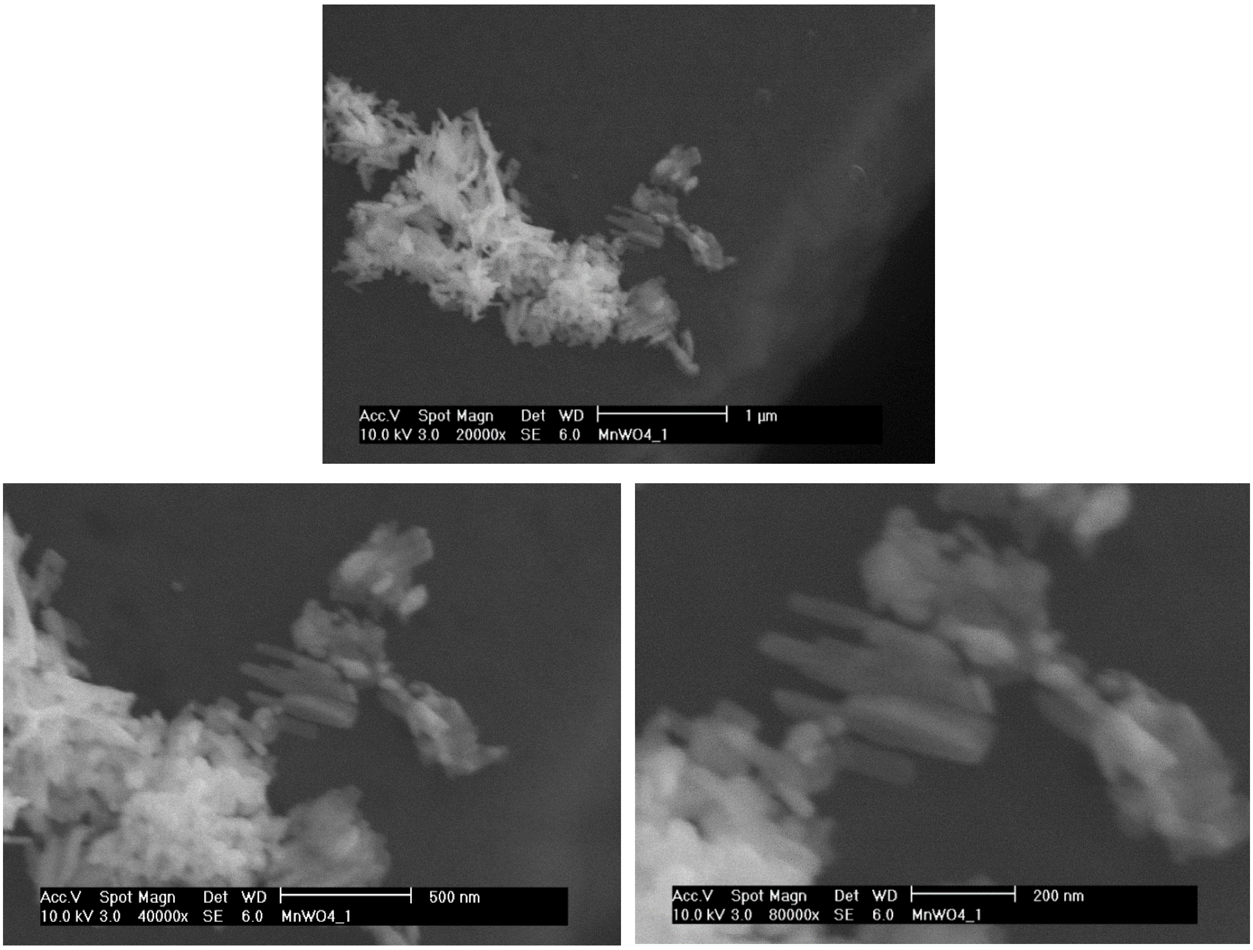

Figure 4.4.1. SEM images of the $MnWO_4$ *in different scale*

The most promising compound $MnWO_4$ was chosen for exploring the shape of the compound by using Scanning Electron Microscopy (SEM). The result reads out that the length of $MnWO_4$ particles vary from 200nm to 300nm. They exhibit the shape of nanorods. (Fig. 4.4.1.)

4.5. Photodegradation measurements

4.5.1 Photodegradation measurements of MWO_4 (M = Cu, Mn, Fe, Ni, Co) synthesized at 400 ℃ in UV light

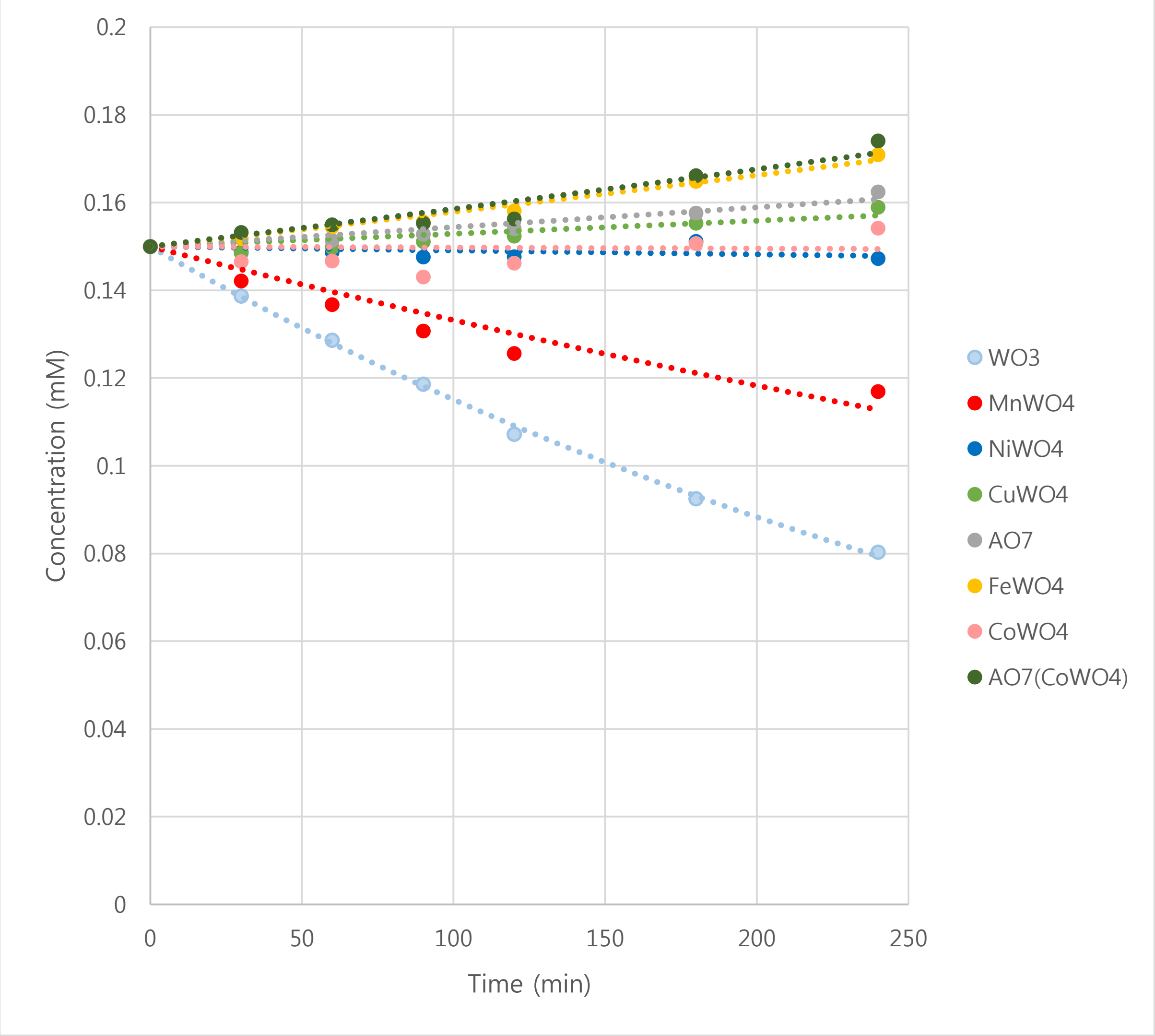

Figure 4.5.1. Photodegradation of 0.15 mM AO7 with MWO_4 (synthesized at 400 ℃) in UV light

Photodegradation performance of the photocatalysts under UV light can be ranked in following order: WO_3 > $MnWO_4$ > $CoWO_4$ ≥ $NiWO_4$ > $CuWO_4$ ≫ $FeWO_4$, which can be seen from figure 4.5.1.

As the time passed by, the temperature of AO7 dye in the box reactor increased due to the intensity of the light. (Table 7.7.1.) Since the solution vaporizes faster due to the increase of temperature, the concentration of the solution arose in general. Also, when comparing different lines of AO7 with photocatalyst and AO7 without photocatalyst in order to observe the photocatalytic activity, different dotted lines/spots of the AO7 line should be compared with corresponding line from AO7 with photocatalyst. For instance, AO7($CoWO_4$) line from the graph should be compared with $CoWO_4$ line. Since 0.15 mM of AO7 solution was prepared each time when it was needed for photodegradation experiment, there are minor difference in concentration from one solution to the other.

In short, under UV light, WO_3 shows the best activity. Overall, $MnWO_4$ is the most promising substance out of the MWO_4 (M = Cu, Mn, Fe, Ni, Co) samples. It is also possible to deduce from the result that $NiWO_4$, $CoWO_4$ and even $CuWO_4$ are photocatalytic active by comparing with inclination of AO7 without any photocatalyst. $FeWO_4$ is the only compound which showed even less photocatalytic activity than the AO7 solution without any catalyst. This is due to the non-crystallinity of the compound as can be seen in Figure 4.1.3.

4.5.2. Photodegradation measurements with WO_3 and MWO_4 (M = Cu, Mn, Ni) impregnated with Pt

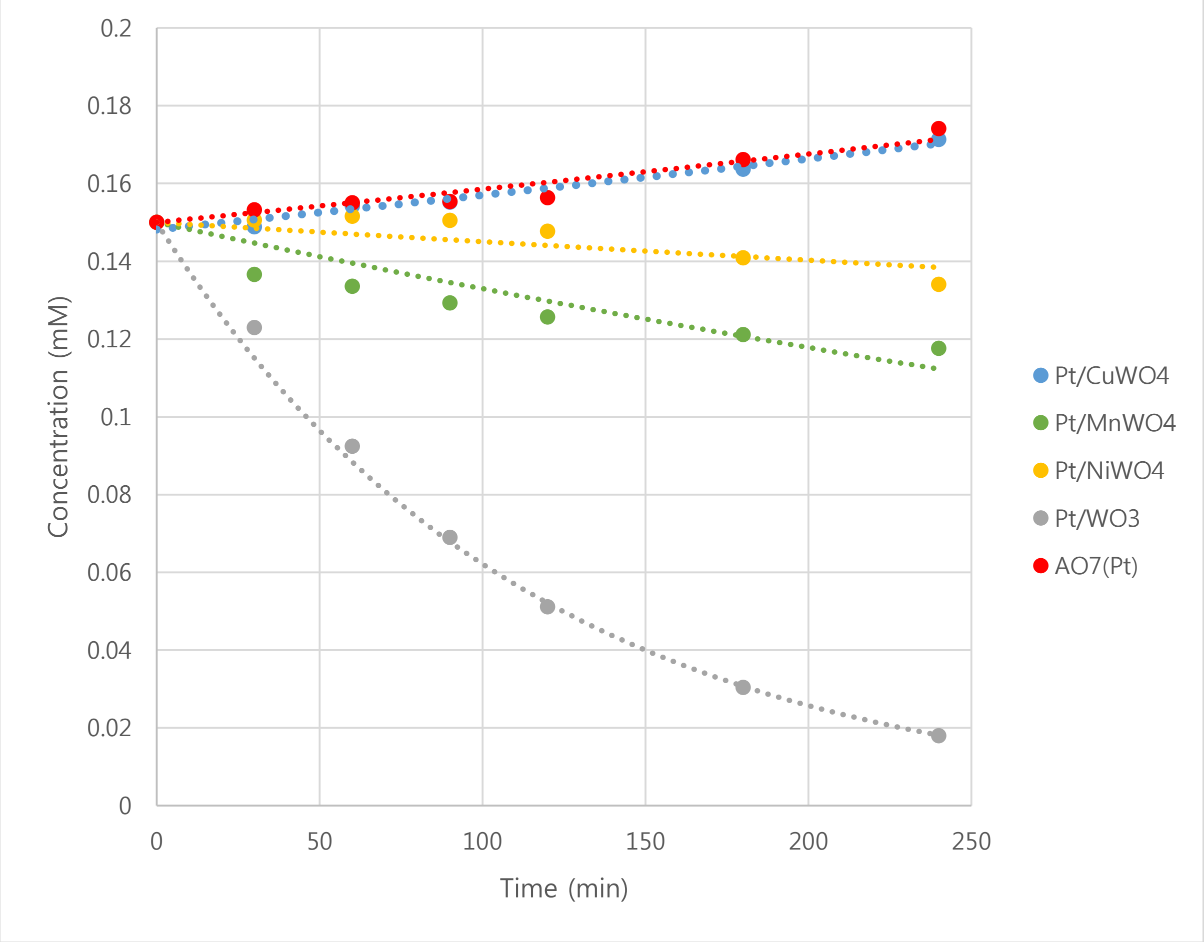

Figure 4.5.2. Photodegradation of 0.15 mM AO7 with MWO_4 (M = Cu, Mn, Ni) and WO_3 which are impregnated with Pt in UV light

The best four compounds which showed photocatalytic activity under UV light with AO7 solution, MWO_4 (M = Cu, Mn, Ni) and WO_3, were chosen. These compounds were impregnated with Pt, which could be working as a cocatalyst. In general, most of the impregnated compounds showed activity under UV light. (Fig. 4.5.2.) WO_3 impregnated with Pt and $NiWO_4$ impregnated with Pt were two samples which showed better activity than the ones without impregnation. $CuWO_4$ and $MnWO_4$, which are impregnated with Pt, are the compounds which show even less activity than the ones without impregnation. Furthermore, $CuWO_4$ is the only compound which showed even less activity than AO7 solution itself when impregnated with Pt.

The amount of dye oxidation increased due to the impregnation of Pt on WO_3.[13] Therefore, higher activity is observed. Hence, impregnation of Pt brings WO_3 with the most advantage when compared with three other compounds.

4.5.3 Photodegradation measurements in visible light under 447 nm spectrum (violet lamp) with and without impregnation of Pt

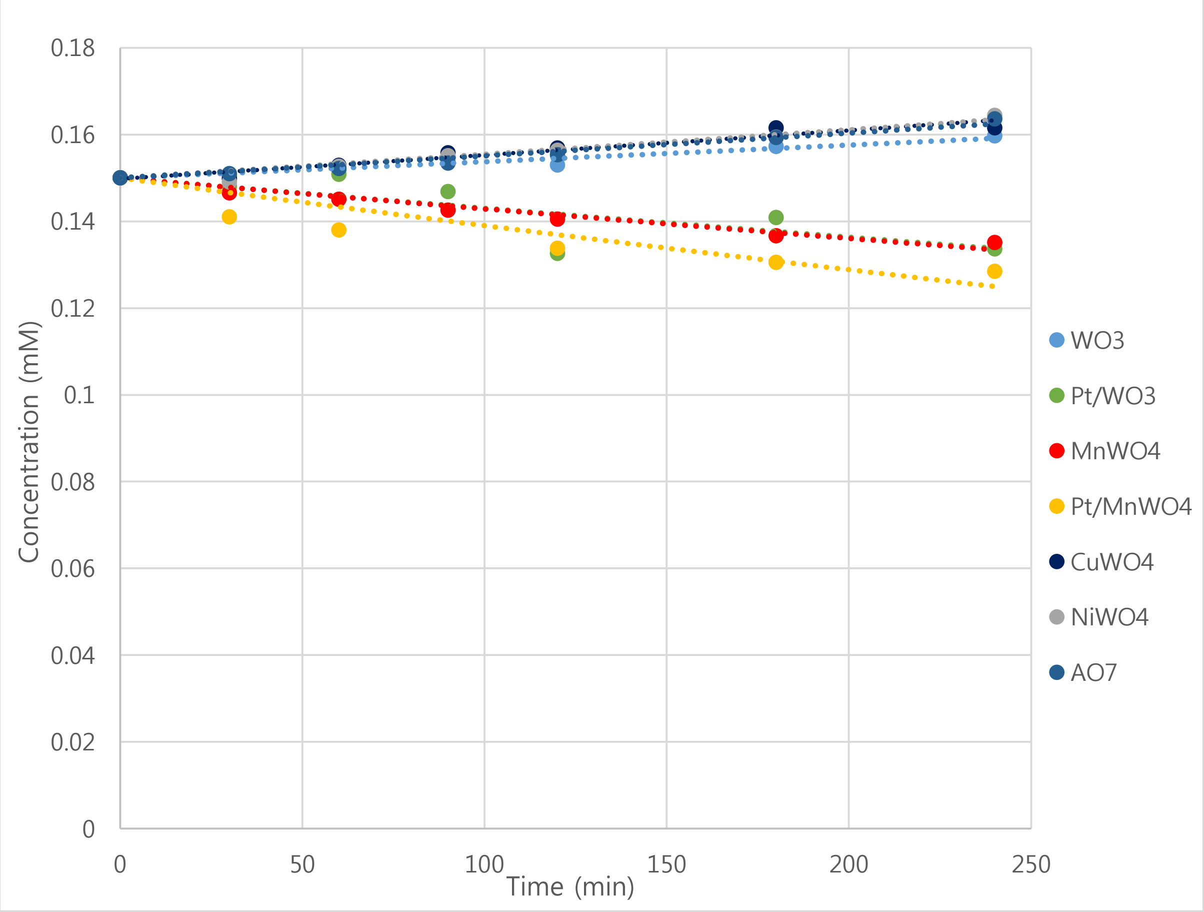

Figure 4.5.3. Photodegradation of 0.15 mM AO7 with the most promising 6 compounds from previous experiments in visible light under 447 nm spectrum (violet lamp)

The most promising 6 samples were chosen from the previous experiments.

Photocatalytic performance in the visible light under 447 nm spectrum can be ranked in following order: Pt/$MnWO_4$ > $MnWO_4$ > Pt/WO_3 ≥ WO_3 ≫ $CuWO_4$ ≥ $NiWO_4$, which can be seen from figure 4.5.3.

As mentioned before, impregnation of Pt was done only on commercial WO_3 and the best three samples, which are $CuWO_4$, $MnWO_4$ and $NiWO_4$. The result was not as promising as the expectation in regards of enhancing the activity under UV light. On the other hand, it enhanced the photocatalytic activity under visible light, for case of WO_3 and $MnWO_4$ compounds.

Here, the result obtained from $MnWO_4$ was fascinating. Compared to WO_3, despite of the fact that it showed less activity in UV light, it was showing more activity in visible light, which was the first aim of the project in general.

4.5.4 Photodegradation measurements with $MnWO_4$ which was calcined at different temperatures (400℃, 550℃ and 700℃)

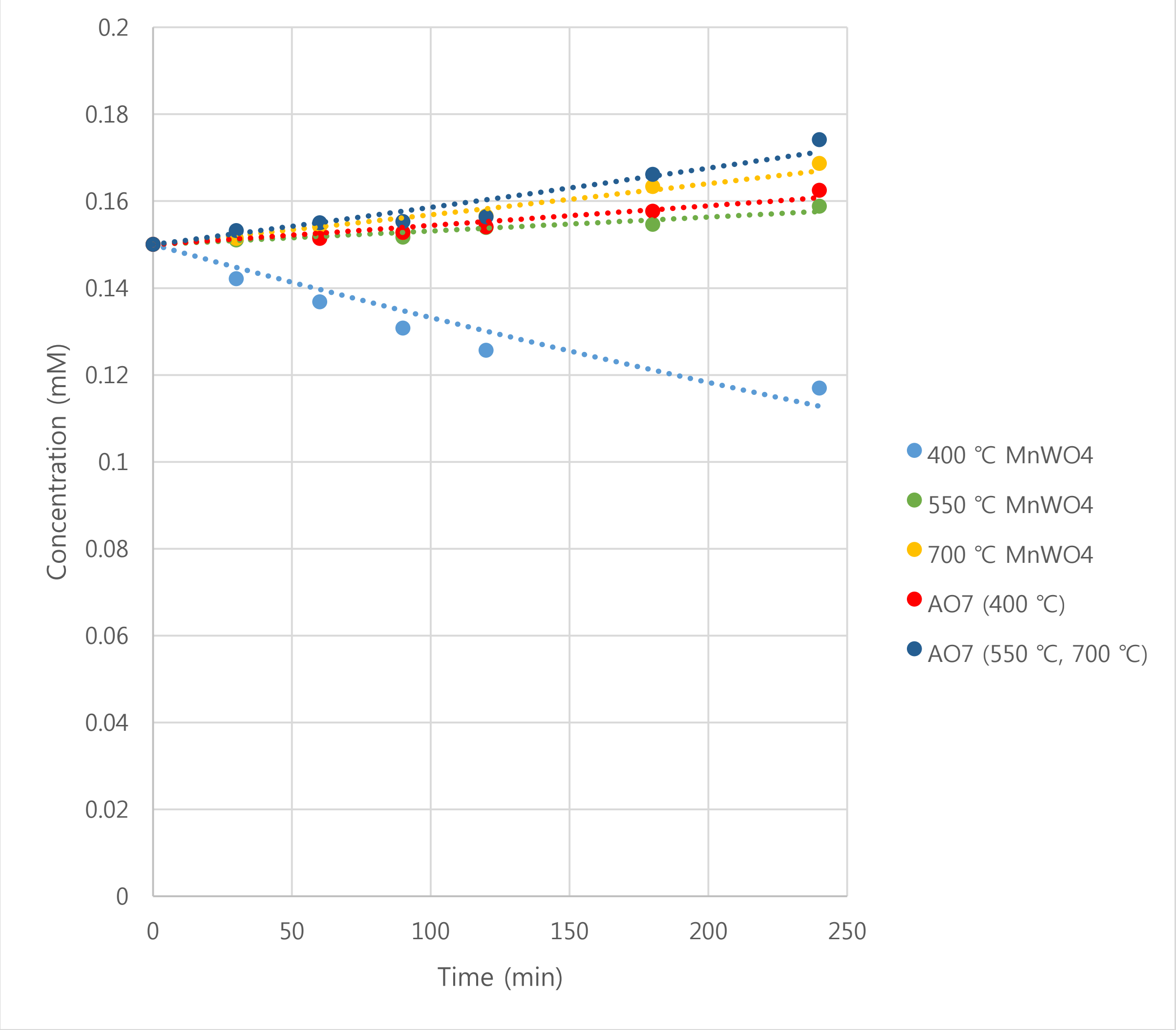

Figure 4.5.4. Photodegradation of 0.15 mM AO7 with $MnWO_4$ samples which were synthesized at different temperatures (at 400℃, 550℃ and 700℃) in UV light

The main point which can be read out from this Figure 4.5.4. is that as the calcination temperature increased, the activity was less for $MnWO_4$. This conclusion might not hold for the other compounds though, since the crystallinity differed within three chosen temperatures when compared with XRD patterns from chapter 4.1.

4.5.5. Other photodegradation experiments

There were two more dye photodegradation experiments which have been explored. One is 'Photodegradation of AO7 in UV light (Synthesized at 700 ℃)' and the other is 'Photodegradation of AO7 with Fe^{3+}'. The results can be found in Appendix chapter 7.4.

In the case of the photodegradation of AO7 with MWO_4 (M = Cu, Mn, Fe, Ni, Co) calcined at 700℃ in UV light, all the photocatalytic activities were decreased significantly apart from $FeWO_4$. (Fig. 7.3.1.) It seems that $FeWO_4$ has gained more crystallinity during the calcination process as one could see from XRD patterns (Fig. 4.1.3.). In order to find out why this happens, measuring the BET surface areas was tried, but this failed due to a defect of the device. This could have led to understand the correlation between calcination temperatures with the surface area of the MWO_4 compounds.

Also photodegradation experiments of AO7 with Fe^{3+}, which would act as an electron scavenger, did not show an interesting result. (Fig. 7.4.1.) For the experiment, two sets of AO7 dye solutions were prepared, one with $Fe^{3+}$and the other without Fe^{3+}. In AO7 photodegradation experiments done with Fe^{3+}, a drastic decrease in reaction rate could be observed. But it was later found that the solution itself without any compounds (MWO_4) was reacting under UV light. Even though the dye itself was reacting, adding Fe^{3+} enhanced the photocatalytic activity on WO_3 and $MnWO_4$.

In the Appendix chapter, one can also see the result of an experiment which was performed the same way as the photodegradation experiments but then without any light. (Fig. 7.2.1.) This was done to check whether AO7 is not degraded due to (non-photo)catalytic effects of the photocatalysts.

5. Conclusion and Recommendation

5.1 Conclusion

The main aim of the research was to investigate the best photocatalyst with band gap smaller than WO_3 with a wider absorption band. The compound $MnWO_4$, which meets with these criteria, has been correctly synthesized. Moreover, $MnWO_4$ was more photocatalytic active than WO_3 under visible light while having less activity under UV light.

In the experiments of dye photodegradation with Pt impregnated on the photocatalysts under UV light, the performance was enhanced for WO_3 and $NiWO_4$. On the other hand, the performance decreased for $MnWO_4$ and $CuWO_4$. However, impregnation of Pt on $MnWO_4$ catalyst improved the photocatalytic activity under visible light. Additionally, when the compounds were calcined at different temperatures, the photocatalytic activity decreased as the temperature was raised.

Rating photocatalytic performance under solar spectrum according to experiments results, the following order can be established: $MnWO_4 \geq WO_3 \gg NiWO_4 \geq CoWO_4 > CuWO_4 \gg FeWO_4$. However, in such a case where different preparation methods are used for the synthesis, different results could be obtained. For instance, in the research of P. Chen, they graded as $FeWO_4 > CoWO_4 > NiWO_4$ in photocatalytic performance under both visible light and sunlight. [1]

As the experiments were done with MnWO4 in this research, conclusion can be reached that an innovative material was found which could be applied in future studies in photocatalysis. In the end, this result could be seen as a small step in leading to an efficient conversion of solar energy into chemical energy. Furthermore, several recommendations are outlined in following chapter in this regard.

5.2 Recommendation

1. When synthesizing MWO_4, it is recommended to calcine samples at several different temperatures and different time durations. Doing a lot of calcination steps would lead to finding the best calcination temperature for finding the best photocatalytically active compound. In this research, better crystallinity was observed as the temperature rose. Unexpectedly, the samples which were calcined at 550 ℃ and 700 ℃ showed less activity in photodegradation experiment.

2. One should measure BET surface area of the compounds. With measuring the BET surface area, getting a correlation between calcination temperatures with the surface area of the MWO_4 compounds can be easily done. The samples which were calcined under 550℃ and 700℃ were sent to be measured in the lab of CPM, but the device was broken under the period while the research was performed.

3. Photodegradation of AO7 with Fe^{3+} ions showed drastic decrease in absorption. AO7 with Fe^{3+} solution was degraded without a catalyst under UV-light, so one could perform the experiment under visible light instead.

4. Now in the field where WO_3 is widely utilized, $MnWO_4$ could be implemented instead and tested. This outcome would bring more options when choosing smaller band gap materials for photocatalytic devices where WO_3 has been incorporated and even further enhancing the sensitivity of the photocatalytic devices towards absorbing light with higher wavelengths. It could be applied for example as one component in a Z-scheme as well which was discussed in the introduction as one of the methods for making a photocatalytic device to split water using visible light.

5. Controlling the morphology of $MnWO_4$ can be done using capping agents. Then, this would lead in understanding the relation between morphology and photocatalytic activity. Recently, research has been done on $MnWO_4$ nanocrystals which were synthesized by a surfactant-free hydrothermal method with different shapes, such as nanospheres, nanorods, and urchin-like microspheres. Wang, Y et al,[14] state that varying the pH. values and precursors would help in understanding the morphologies of $MnWO_4$ nanocrystals.[14] Photodegradation experiment has not been done yet for these various types of $MnWO_4$. In short, after synthesizing $MnWO_4$ with different morphologies, AO7 photodegradation experiments with these different samples could be performed to find out if there is a relationship between morphology and photocatalytic activity.

6. It seems that the $CoWO_4$ has as good photocatalytic activity as $NiWO_4$. (Fig. 4.1.3.) Since it was synthesized at the end of the project, further experiments with and without impregnation of Pt under UV light and visible light would be recommended to be performed.

6. Bibliography

(1) Chen, P.; He, H. Y. *Research on Chemical Intermediates* **2013**.

(2) García-Pérez, U. M.; Martínez-De La Cruz, A.; Peral, J. *Electrochimica Acta* **2012**, *81*, 227.

(3) Rajagopal, S.; Nataraj, D.; Khyzhun, O. Y.; Djaoued, Y.; Robichaud, J.; Mangalaraj, D. *Journal of Alloys and Compounds* **2010**, *493*, 340.

(4) Montini, T.; Gombac, V.; Hameed, A.; Felisari, L.; Adami, G.; Fornasiero, P. *Chemical Physics Letters* **2010**, *498*, 113.

(5) A, L. *Progress in PVs; Research and Applications* **2001**.

(6) T, B. *Renewable Energy* 1999.

(7) Bloch, P. **1995**.

(8) Michel G. C. Zoontjes, M. H., Jonas Baltrusaitis, Wilfred G. van der Wiel, and Guido Mul* *ACS, Applied Materials & Interfaces* **2013**.

(9) Li, Q., Guo, B., Yu, J., Ran, J., Zhang, B., Yan, H., & Gong, J. R. *Journal of the American Chemical Society* **2011**, 133(28).

(10) Maeda, K. *Journal of Photochemistry and Photobiology C: Photochemistry Reviews* **2011**, *12*, 237.

(11) Hagens, N. In *The Oil Drum*; 01/07 ed. 2009.

(12) Janáky, C.; Rajeshwar, K.; de Tacconi, N. R.; Chanmanee, W.; Huda, M. N. *Catalysis Today* **2013**, *199*, 53.

(13) Abe, R.; Takami, H.; Murakami, N.; Ohtani, B. *Journal of the American Chemical Society* **2008**, *130*, 7780.

(14) Wang, Y.; Yang, L.; Wang, Y.; Wang, X.; Han, G. *Ceramics International* **2014**, *40*, 5085.

(15) Catholic Schools Diocese of Maitland-Newcastle 2002.

(16) PANalytical; 2014 ed.; PANalytical, Ed. PANalytical, 2014.

(17) Atkins, P. *Physical Chemistry*, 9 ed. Oxford, 2010.

(18) Cambridge Forecast Group In *Research, Science & Technology*, Cambridge Forecast Group, Ed. 2006.

(19) SHIMADZU; No.A428, S. A., Ed.; SHIMADZU CORPORATION: Chiyoda-ku, Tokyo.

(20) TECHNOLOGIES, P. **2011**.

(21) Szilágyi, I.; Santala, E.; Heikkilä, M.; Kemell, M.; Nikitin, T.; Khriachtchev, L.; Räsänen, M.; Ritala, M.; Leskelä, M. *J Therm Anal Calorim* **2011**, *105*, 73.

7. Appendix

7.1. Tauc plots of $MnWO_4$, WO_3, $NiWO_4$ and $FeWO_4$ with Kubelka-Munk spectra of $MnWO_4$, WO_3

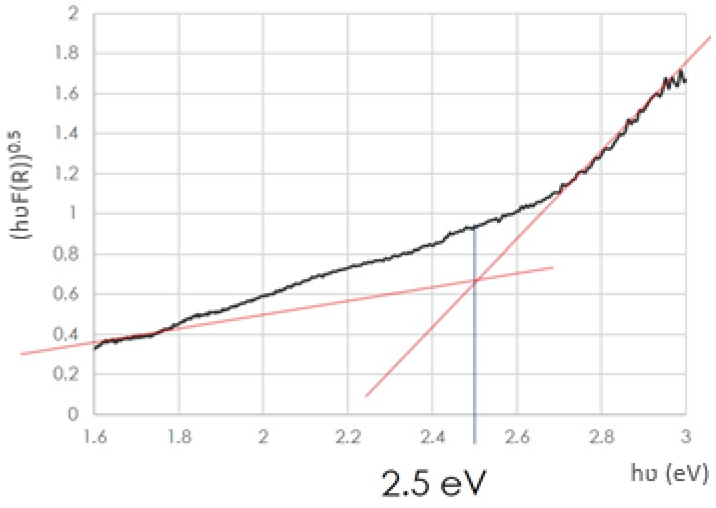

Figure 7.1.1. Tauc Plot of $MnWO_4$

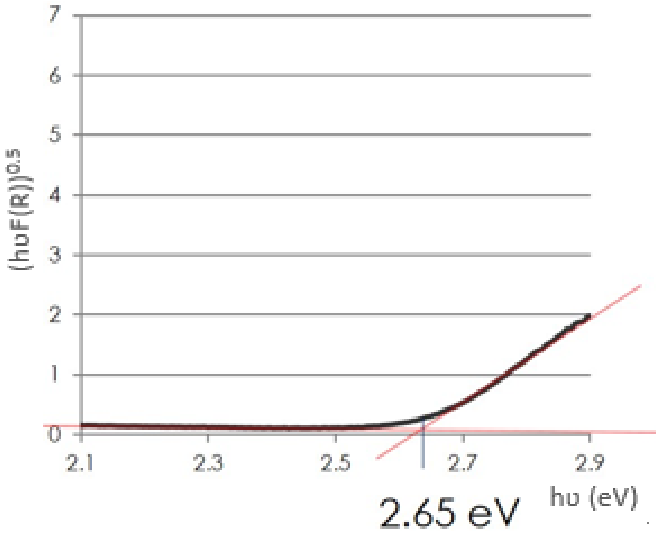

Figure 7.1.2.Tauc Plot of WO_3

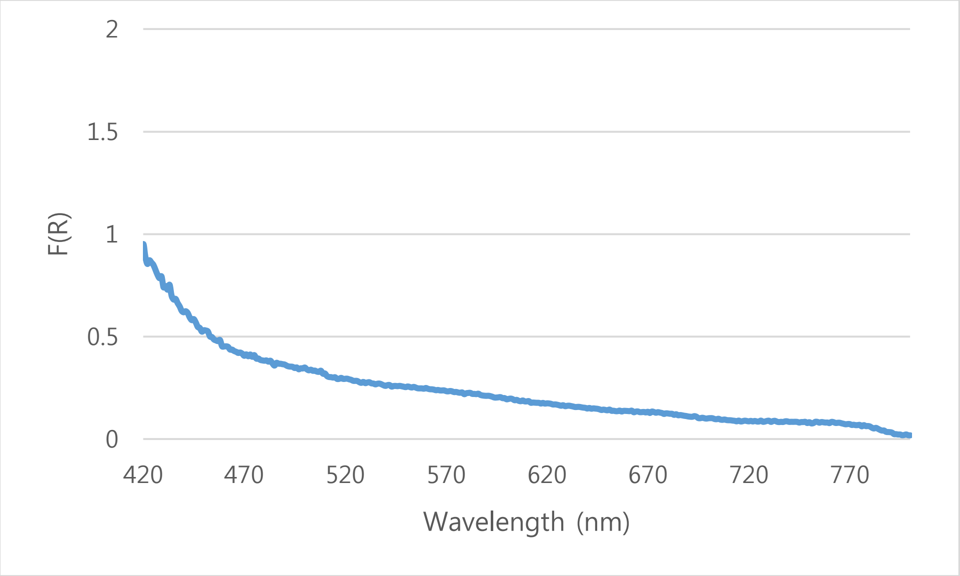

Figure 7.1.3. Kubelka-Munk plot of $MnWO_4$

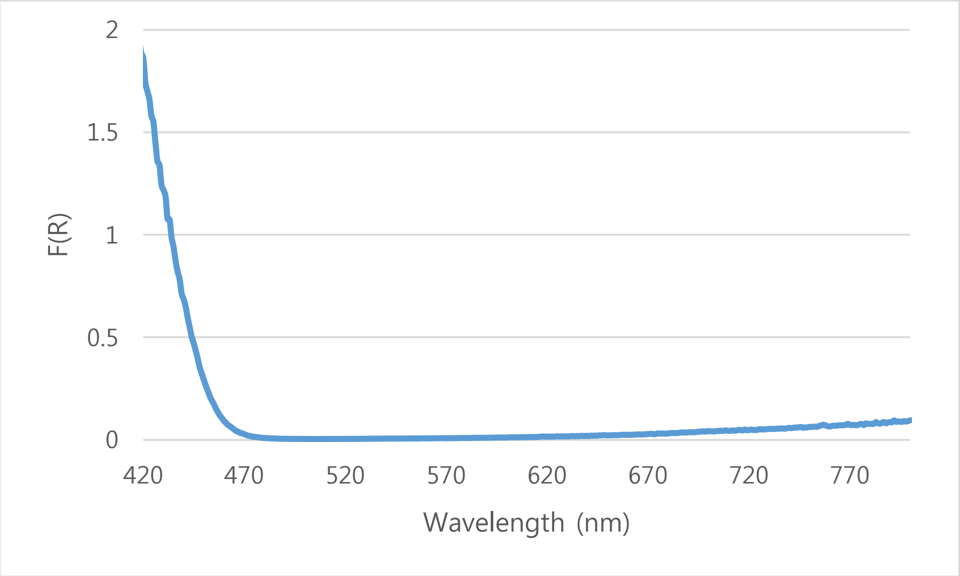

Figure 7.1.4. Kubelka-Munk plot of WO_3

Kubelka-Munk plots tell us how it is responding to UV/visible light. By comparing two figures (Fig. 7.1.3. and Fig. 7.1.4.), it can be deduced that $MnWO_4$ can absorb light with a higher wavelength than WO_3.

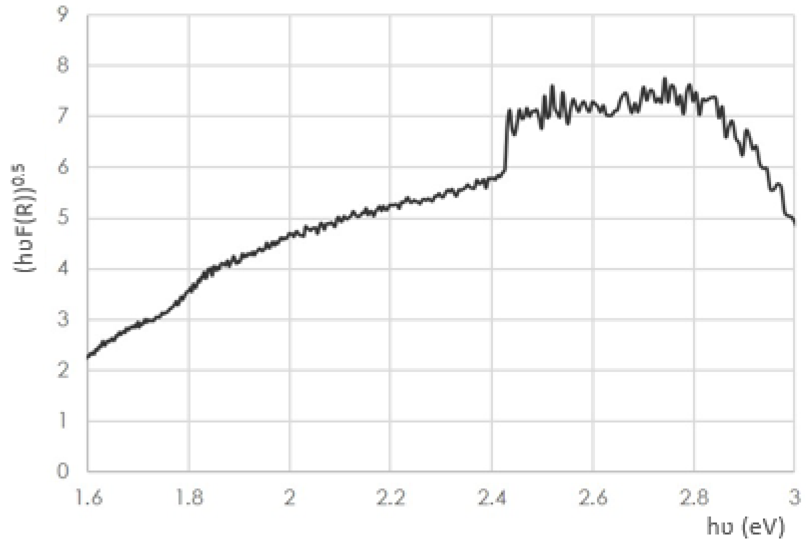

Figure 7.1.5. Tauc Plot of $FeWO_4$

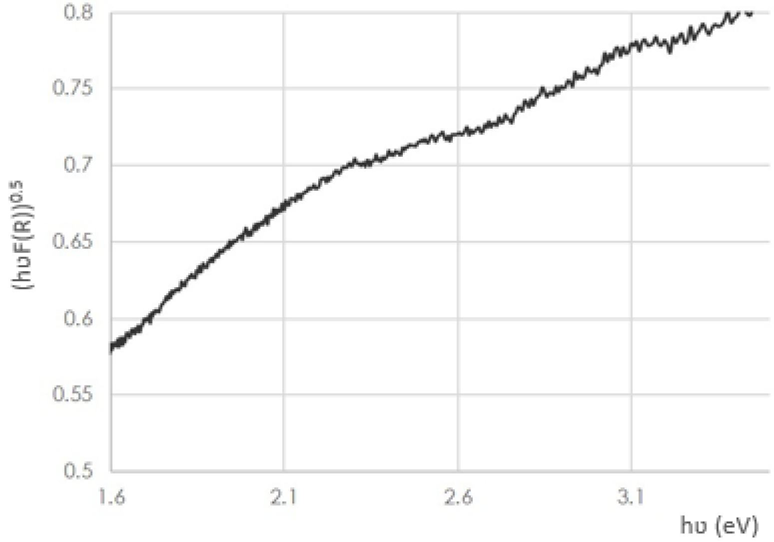

Figure 7.1.6. Tauc Plot of $NiWO_4$

7.2. Degradation in the dark?

This experiment was not only done to prove that the MWO_4 (M = Cu, Mn, Fe, Ni, Co) are photocatalytic active, but also to prove that AO7 with Fe^{3+} solution itself was not reacting in the dark, but under UV light.

Experiments were done to observe if AO7 reacts with Fe^{3+} in the dark. The graph on the top is with the most promising substance $MnWO_4$, and the other one on the bottom is AO7 with Fe^{3+}.

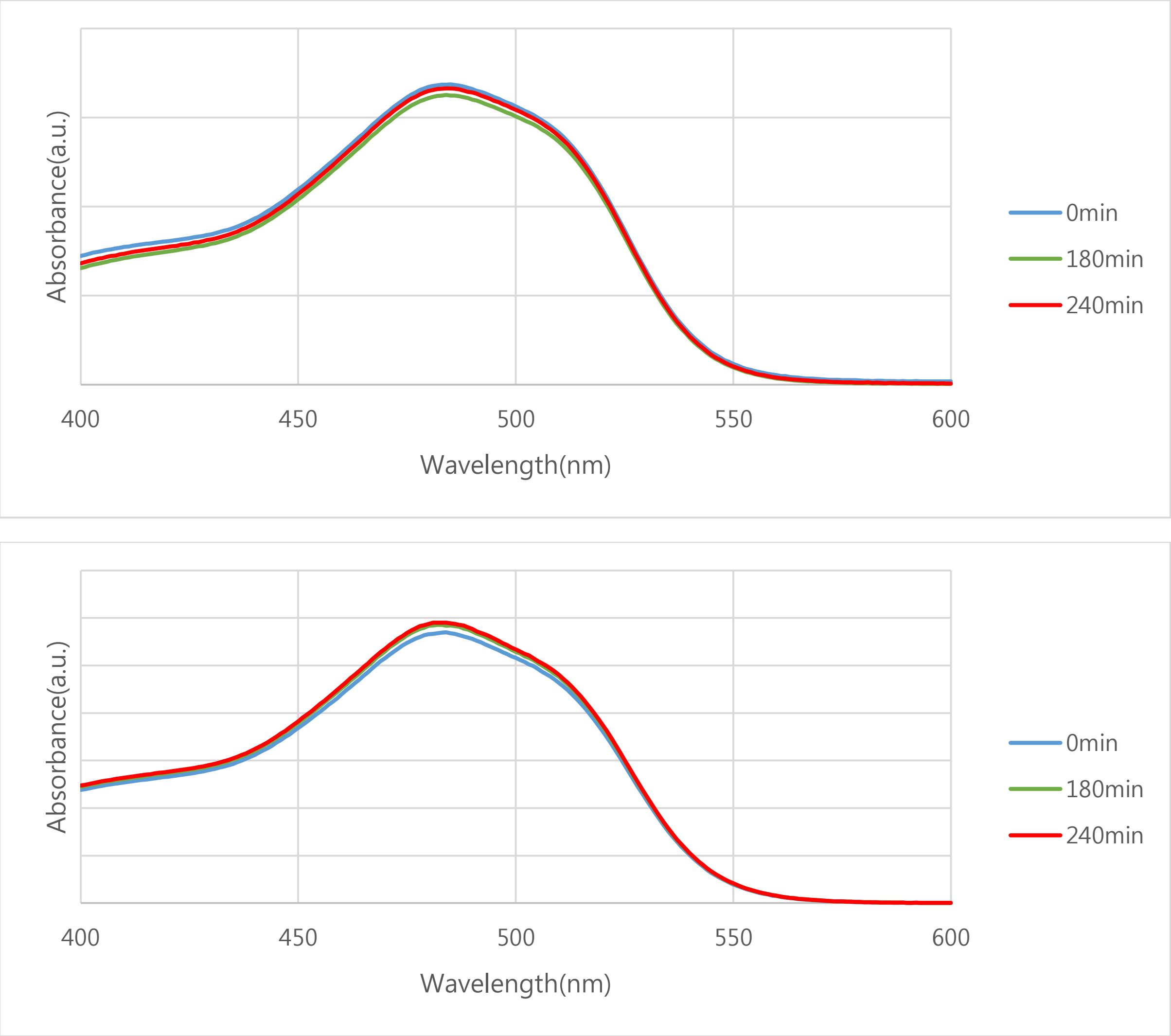

Figure 7.2.1. Absorbance spectra of 0.15mM AO7 solution with $MnWO_4$ *in dark (top) and same solution with* Fe^{3+} *(bottom)*

7.3. Photodegradation measurement in UV light with MWO_4 (M = Cu, Mn, Fe, Ni, Co) which was synthesized at 700 ℃.

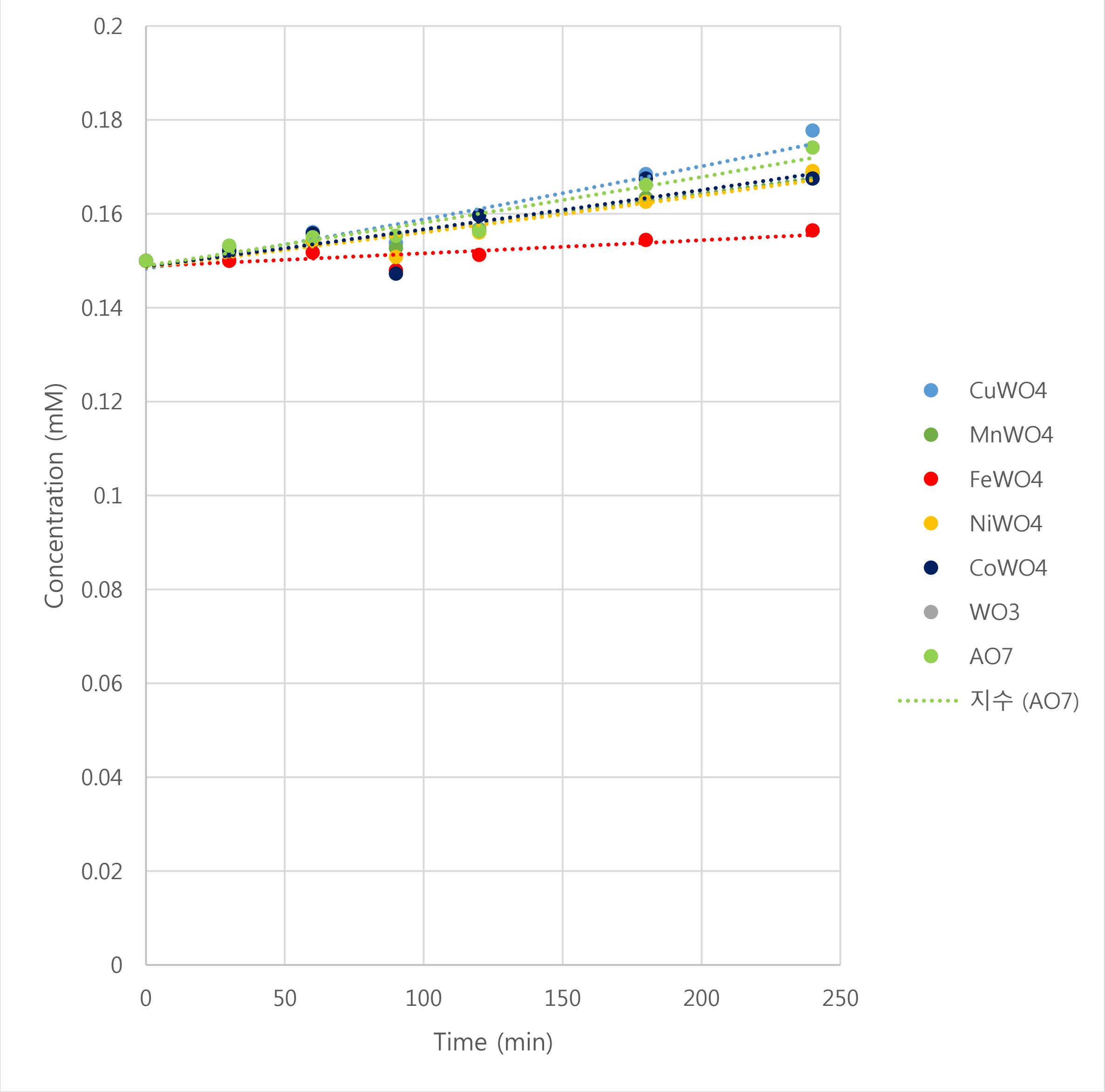

Figure 7.3.1. Photodegradation of 0.15mM AO7 solution with MWO_4 samples (treated at 700 ℃) in UV light

7.4. Photodegradation of AO7 with Fe^{3+}

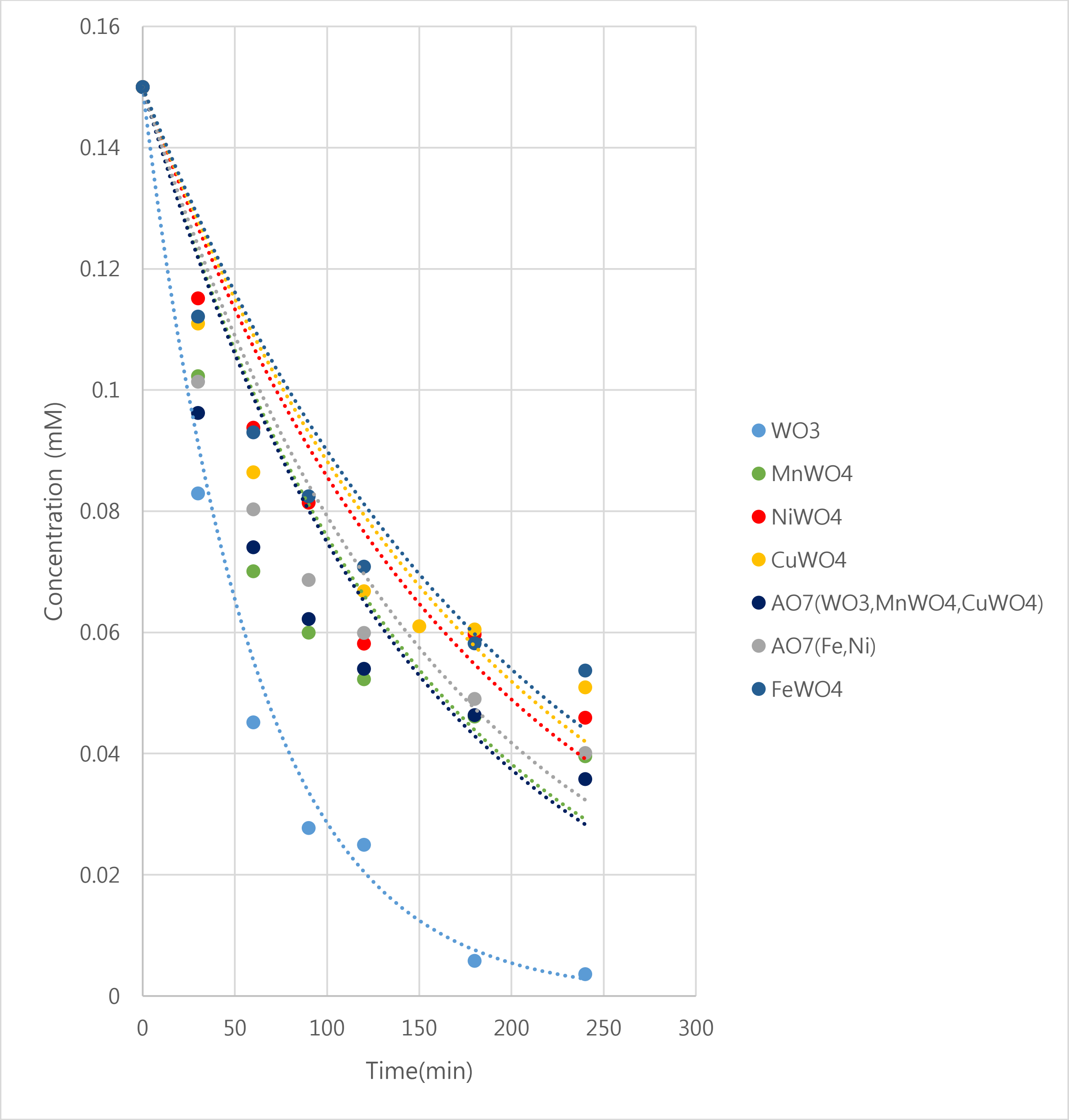

Figure 7.4.1. Photodegradation of 0.15mM AO7 with Fe^{3+} in UV light

7.5. XRD pattern of $FeWO_4$ when synthesized by a co-precipitation method.

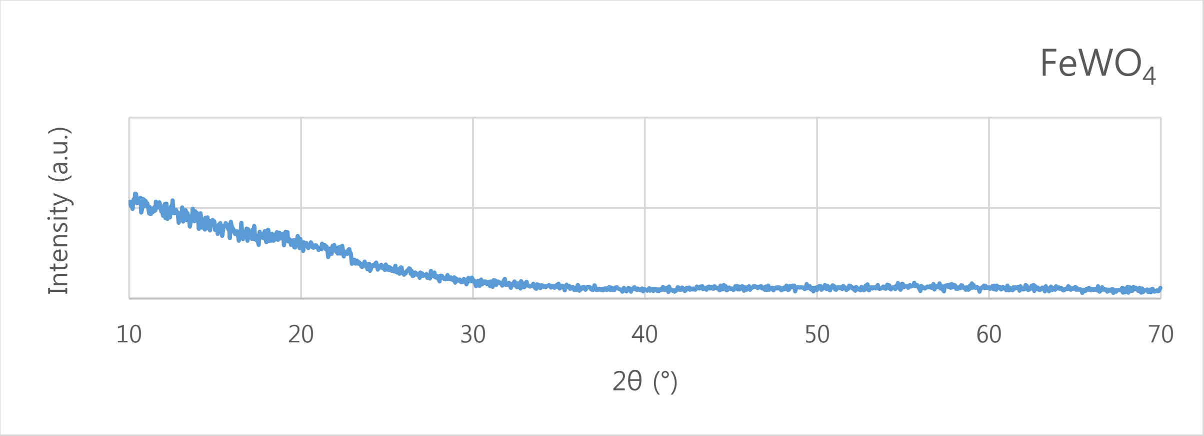

Figure 7.5.1. XRD pattern of $FeWO_4$, when synthesized by a co-precipitation method.

This sample is not crystalline and therefore it is difficult to see peaks in this XRD pattern.

7.6. Photodegradation measurements of 4.5.3 and 4.5.4 combined

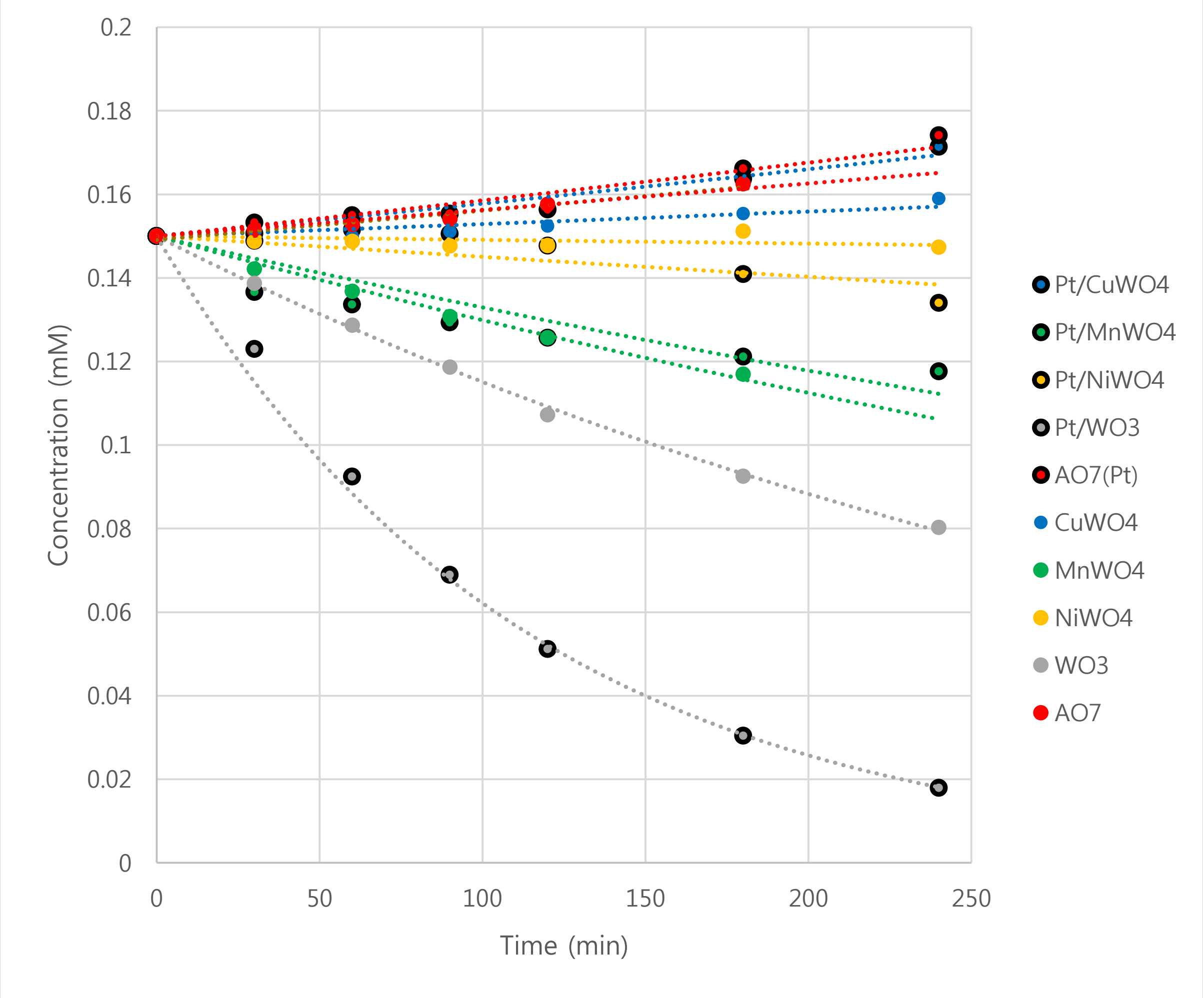

Figure 7.6.1. Comparison of two experiments (with and without impregnation of Pt) of photodegradation of 0.15 mM AO7 with MWO_4 (M = Cu, Mn, Ni) and WO_3 in UV light. Dots with a black border correspond to samples impregnated with Pt. Dots without any border color correspond to the samples without impregnation.

7.7. Increase in temperature of AO7 dye in the box reactor

Time (min)	0	30	60	90	120	180	240
Temperature (℃)	20.6	24.1	26.3	27.7	28.3	29.8	30.1

Table 7.7.1. Increase in temperature of AO7 dye in the box reactor during photodegradation experiment in UV light

7.8. Table of steps for synthesizing MWO_4 (M = Cu, Mn, Fe, Ni, Co)

Normal synthesis of MWO_4 (M = Cu, Mn, Fe, Ni, Co) takes 3 days. The first day, it takes an hour and a half to dissolve the solutions and combine them. After centrifuging three times with the centrifuging machine, which also takes an hour and a half, the substances are put into a drying oven for 24h at 90 ℃. Right after drying, the materials are put into a calcination oven for another 24h at 400 ℃.

<table>
<tr><th></th><th>$CuWO_4$</th><th>$MnWO_4$</th><th>$FeWO_4$</th><th>$NiWO_4$</th><th>$CoWO_4$</th></tr>
<tr><td>Quantity of Solution A</td><td>$CuCl_2\cdot 2H_2O$ 0.00963 mol (1.6417g) + 15mL of distilled water</td><td>$MnCl_2\cdot 4H_2O$ 0.00963 mol (1.9059) + 15mL of distilled water</td><td>$FeSO_4\cdot 7H_2O$ 0.00963 mol (2.6772g) + 15mL of distilled water</td><td>$Ni(NO_3)_2\cdot 6H_2O$ 0.00963 mol (2.8003g) + 15mL of distilled water</td><td>$CoCl_2\cdot 6H_2O$ 0.00963 mol (2.2912g) + 15mL of distilled water</td></tr>
<tr><td>Quantity of Solution B</td><td colspan="5">$Na_2WO_4\cdot 2H_2O$ 0.00963 mol (3.1765g) + 25mL of distilled water</td></tr>
<tr><td colspan="6">Solution A and Solution B are stirred for 20 min. (300 RPM~350 RPM)
A was added drop wise into B under stirring. (300 RPM~500 RPM)
The desired solution is then stirred for 20 min to 3 hours.</td></tr>
<tr><td>$FeWO_4$</td><td colspan="5">$FeWO_4$ is the only material which was synthesized using a hydrothermal synthesis method. It is put into a Teflon-lined autoclave at 180 ℃ for 12 hours.</td></tr>
<tr><td colspan="6">Perform centrifuging 3 times in 8500 rpm for 30 min first with the solution, then 20 min with millipore water and then another 20 min with ethanol.</td></tr>
<tr><td colspan="6">Put the sample in the ceramic bowl for drying. Drying is done at 90 ℃ for 24 hours.</td></tr>
<tr><td>$CuWO_4$, $MnWO_4$, $NiWO_4$, $CoWO_4$</td><td colspan="5">After drying, calcination of the samples is done at 400 ℃ for 24 hours.</td></tr>
<tr><td colspan="6">Grind and store the sample.
Perform XRD to see if the graph corresponds to the literature.
Reproduce once again with following the same procedure to double check.</td></tr>
</table>

7.9. Experiment footage

	Monday	Tuesday	Wednesday	Thursday	Friday
Week 1 (11~15/11)	-	(Started) Synthesis of $CuWO_4$	Dye degradation practice	grind & store the sample	XRD with $CuWO_4$ *Shell Workshop*
Week 2 (18~22/11)	Synthesis of $MnWO_4$ & $FeWO_4$		*Practicum Nano filtration*		
Week 3 (25~29/11)			Re-Synthesis of $CuWO_4$		
Week 4 (2~6/12)	Feedback from Kasper. Synthesis of $CuWO_4$, $MnWO_4$, $FeWO_4$		Calcination *Meeting for project*	grind & store the sample *Meeting for project*	XRD $CuWO_4$, $MnWO_4$, $FeWO_4$
Week 5 (9~13/12)	Synthesis of $CuWO_4$, $MnWO_4$, $NiWO_4$	Prepare Solution for photo dyegradation , Synthesis of $FeWO_4$	photo dyegradation	XRD $NiWO_4$, $FeWO_4$ Measure band gaps for $MnWO_4$, $CuWO_4$	*Presentation Nano filtration*
Week 6 (16~20/12)	Band gap determination	Work out results Re-$MnWO_4$, $NiWO_4$ synthesis	AO7 photo dyegradation $NiWO_4$ and $FeWO_4$ (with and without Fe3+)	AO7 photo dyegradation With most promising 4 samples XRD	AO7 photo dyegradation in dark

Week 7 (6~10/1)	-		Impregnation of Pt on MnWO4 and CuWO4	grind & grind the sample	Raman spectroscopy & SEM
Week 8 (13~17/1)				Midway Presentation	-WO$_3$ impregnation -Prepare 3 sets each from MWO$_4$ for calcination(550, 700, best) -Band gap Remeasurements -Calcination in 700 with normal samples (100 mg)
Week 9 (20~24/1)	- Synthesis of CoWO$_4$ -NiWO$_4$ impregnation -BET. go to other lab(1) -Calcination in 550 with normal samples (100 mg)	-Calcination for impregnation of NiWO$_4$,WO$_3$ & Synthesis -XRD for the calcination 550&700	- XRD for CoWO$_4$ Photodegradation with MWO$_4$ in visible light		**EXAM** Band gap Remeasurements (On best result one)
Week 10 (27~31/1)	Calcination in best temp. with normal samples (150 mg) Photodegradation with		**EXAM**	Photodegradation with MWO$_4$ impreganted with Pt in visible light	Photodegradation with CoWO$_4$(with MnWO$_4$ for comparison) in UV light

	MWO_4 impreganted with Pt in UV				
Week 11 (3~7/2)					
Week 12 (10~14/2)	Finish up Experiment this week	Capping Agent	-BET. go to other lab. (2)		
Week 13~ Week 21 (17/2~4/4)	Write a report, first draft till 4th of April				
Week 22 (7/4~11/4)	Finish up the report and preparation for Final Presentation				
17/4	Final Defense				